

Cesar Augusto Conopoima Pérez

**Mortar Finite Element Method for cell response to applied electric field**

Dissertação apresentada ao Programa de Pós-graduação em Modelagem Computacional, da Universidade Federal de Juiz de Fora como requisito parcial à obtenção do grau de Mestre em Modelagem Computacional.

Orientador: Prof. D.Sc. Bernardo Martins Rocha

Coorientador: Prof. D.Sc. Rodrigo Weber Dos Santos

Coorientador: Prof. D.Sc. Iury Higor Aguiar Da Igreja

Juiz de Fora

2017

Ficha catalográfica elaborada através do programa de geração automática da Biblioteca Universitária da UFJF, com os dados fornecidos pelo(a) autor(a)

Conopoima Pérez, Cesar Augusto.

Mortar Finite Element Method for cell response to applied electric field / Cesar Augusto Conopoima Pérez. -- 2017.

69 p. : il.

Orientador: Bernardo Martins Rocha

Coorientadores: Rodrigo Weber dos Santos, Iury Higor Aguiar da Igreja

Dissertação (mestrado acadêmico) - Universidade Federal de Juiz de Fora, ICE/Engenharia. Programa de Pós-Graduação em Modelagem Computacional, 2017.

1. Mortar Finite Element Method. 2. Lagrange multiplier. 3. Passive and active response of the cell. 4. Applied electric field. I. Martins Rocha, Bernardo, orient. II. Weber dos Santos, Rodrigo, coorient. III. Aguiar da Igreja, Iury Higor, coorient. IV. Título.

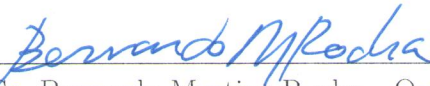
Cesar Augusto Conopoima Pérez

Mortar Finite Element Method for cell response to applied electric field

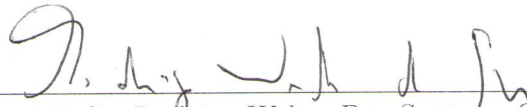
Dissertação apresentada ao Programa de Pós-graduação em Modelagem Computacional, da Universidade Federal de Juiz de Fora como requisito parcial à obtenção do grau de Mestre em Modelagem Computacional.

Aprovada em 25 de Setembro de 2017.

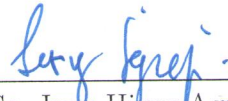
BANCA EXAMINADORA



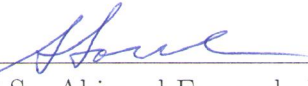
Prof. D.Sc. Bernardo Martins Rocha - Orientador  
Universidade Federal de Juiz de Fora



Prof. D.Sc. Rodrigo Weber Dos Santos - Coorientador  
Universidade Federal de Juiz de Fora



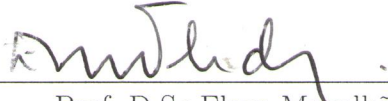
Prof. D.Sc. Iury Higor Aguiar Da Igreja - Coorientador  
Universidade Federal de Juiz de Fora



Prof. D.Sc. Abimael Fernando Dourado Loula  
Laboratório Nacional de Computação Científica



Prof. D.Sc. Grigori Chapiro  
Universidade Federal de Juiz de Fora



Prof. D.Sc. Elson Magalhães Toledo  
Laboratório Nacional de Computação Científica

*To the nature.*

## ACKNOWLEDGEMENTS

First of all I would like to thank to the Pos-graduate Program in Computational Modelling of the Federal University of Juiz de Fora, for choosing me as international student in the program, I also thank to all the professors which I meet and have fruitful discussions during the master courses, specially I would like to thank professor Bernardo Martins Rocha by allowing me to work over his nicely constructed FEM library (cardiax). I also thank him for his guidance and patience, every meeting was a profitable time that allow this work to be finished; to professor Iury da Igreja by the hours of informal discussion about The Finite Elements Method, they were certainly very useful to conclude this work; to professor Rodrigo Weber dos Santos also by his guidance and for the informal talks about everything, in particular about electrophysiology, his insights and knowledge truly enriched this work.

I am also very thankful to all the friends in the laboratory, some for making the coffee break an enjoyable time, and others for the interesting chatting about they research works. I am grateful to all the Brazilians, specially to the Mineiros, that I encounter and lived during this time in Brazil, they make me feel authentically welcome in their country, all the personal and professional growth I experience in the past year was only possible thanks to them. Finally I am very grateful to Marissa Scárdua by her patient and help in difficult times, her unmeasurable kindness and love inspire me every day.

To CAPES for the financial support during the development of this work and during the complete master course.

## ABSTRACT

The response of passive and active biological cell to applied electric field is investigated with a Mortar Finite Element Method MFEM. Cells response is a process with two different time scales, one in microseconds for the cell polarization and the other in milliseconds for the active response of the cell due to the complex dynamics of the ion-channel current on the cell membrane. The mathematical model to describe the dynamics of the cell response is based on the conservation law of electric current in a conductive medium. By introducing an additional variable known as Lagrange multiplier defined on the cell interface, the boundary value problem associated to the conservation of electric current is decoupled from the initial value problem associated to the passive and active response of the cell. The proposed method allows to solve electric potential distribution in arbitrary cell geometry and arrangements. In order to validate the presented methodology, the h-convergence order of the MFEM is numerically investigated. The numerical and exact solutions describing cell polarization are also compared. Finally, to demonstrate the effectiveness of the method, the active response to an applied electric field in cells clusters and cells with arbitrary geometry are investigated.

**Key-words:** Mortar Finite Element Method. Lagrange Multiplier. Passive and active response of the cell. Applied electric field.

## RESUMO

A resposta passiva e ativa de uma célula biológica a um campo elétrico é estudada aplicando um Método de Elementos Finitos Mortar MEFM. A resposta de uma célula é um processo com duas escalas temporais, o primeiro na escala de microsegundos para a polarização da célula e o segundo na escala de milisegundos para a resposta ativa devido a dinâmica complexa das correntes nos canais iônicos da membrana celular. O modelo matemático para descrever a dinâmica da resposta celular é baseado na lei de conservação de corrente elétrica em um meio condutor. Introduzindo uma variável adicional conhecida como multiplicador de Lagrange definido na interface da célula, o problema de valor de fronteira associado a conservação de corrente elétrica é desacoplado do problema de valor inicial associado a resposta passiva e ativa da célula. O método proposto permite resolver o problema da distribuição de potencial elétrico em um arranjo geométrico arbitrário de células. Com o objetivo de validar a metodologia apresentada, a convergência espacial do método é numericamente investigada e a solução aproximada e exata que descreve a polarização de uma célula, são comparadas. Finalmente, para demonstrar a efetividade do método, a resposta ativa a um campo elétrico aplicado num arranjo de células de geometria arbitrária é investigada.

**Palavras-Chaves:** Método de Elementos Finitos Mortar. Multiplicador de Lagrange. Resposta ativa e passiva da célula. Campo elétrico aplicado.

## CONTENTS

1	Introduction .....	14
1.1	Interface problems by FEM .....	15
1.2	Objectives .....	17
1.3	Structure of the work .....	17
2	Biological response of cell to applied electrical field.....	18
2.1	Mathematical models .....	18
2.1.1	<i>Model for electric response of a cell.....</i>	20
2.1.2	<i>The Hodgkin-Huxley model.....</i>	22
3	The Mortar Finite Element Method.....	26
3.1	Preliminaries .....	26
3.1.1	<i>Linear variational formulation problems of one field.....</i>	27
3.1.2	<i>Linear mixed variational formulation problems.....</i>	28
3.2	The model problem .....	31
3.2.1	<i>Existence and uniqueness of the saddle point problem .....</i>	34
3.3	Finite element discretization .....	35
3.3.1	<i>The mortar finite element discretization .....</i>	37
3.3.2	<i>Error estimate .....</i>	39
3.4	Time discretization for the transmembrane current .....	40
4	Computational aspects of the Saddle Point Problem.....	42
4.1	Structure of the indefinite linear system .....	42
4.2	Numerical methods to solve saddle point problems .....	44
4.2.1	<i>Schur Complement.....</i>	44
4.2.2	<i>Penalty method .....</i>	46
4.2.3	<i>Krylov space method .....</i>	47
5	Results .....	48
5.1	h-convergence of the method .....	48
5.2	Exact and numerical solution of the cell interface problem .....	51



5.3	Complex dynamics of the ion current and action potential .....	56
6	Conclusions .....	62
6.1	Future works .....	63
	REFERENCES .....	64

## LIST OF FIGURES

2.1	A circular cell in a conductive medium . . . . .	20
2.2	Polar reference system used in the exact solution. . . . .	22
2.3	Transmembrane potential following the action potential described the Hodgkin-Huxley model for an applied current $I_m = 5[\mu\text{A} \cdot \text{cm}^{-2}]$ and activation variables of the ions channels. . . . .	25
3.1	A circular cell in a conductive medium . . . . .	31
3.2	A general non overlapping domain decomposition . . . . .	37
3.3	A domain decomposition that does not generate vertex . . . . .	37
3.4	Triangulation in two non-overlapping domains and Lagrange multiplier triangulation defined on the non mortar side interface . . . . .	39
3.5	Triangulation of the Lagrange multiplier on the interface, and hat functions for interpolation of the approximated Lagrange multiplier. . . . .	39
4.1	Sparsity pattern of the linear system associated to a discretization with triangular linear elements (161 nodes). Square matrix ( $177 \times 177$ ) with 929 non-zero entries and a maximum number of entries per row of 7. . . . .	43
5.1	Computational domain and numerical solution of the second order interface problem. . . . .	49
5.2	Domain discretization by triangular linear finite elements, matching discretization left and non-matching discretization at right. . . . .	49
5.3	h-convergence study for the primal variable and the Lagrange multiplier for a triangular discretization with matching elements. . . . .	50
5.4	At left the circular cell and the reference system used in the exact solution, at top right the electric potential inside and outside the cell as function of the radius $r$ for a fixed angle $\theta = 0$ ; on the bottom right the transmembranic potential $V_m = u_i - u_e$ defined on the cell interface as a function of the angular position $\theta \in [0, 360]$ . . . . .	51
5.5	Transmembrane current in time. . . . .	52
5.6	A circular cell in a conductive medium . . . . .	53

5.7	Cell domain discretization with triangular elements. . . . .	53
5.8	Reference system of the circular cell to plot the numerical and exact solution. . . . .	54
5.9	Electric potential in function of the angle evaluated at the membrane for the passive response of the cell with matching grids. Exact solution is plotted as continuous functions, and the numerical results are plotted as the dotted lines. . . . .	54
5.10	Left: steady state iso-potential contour around the cell. Right: the domain discretization by triangular elements used to solve the polarization process in the isolated cell. The distance between electrodes is 0.01[cm], the applied electric field is $\mathbf{E} = 5[V \cdot \text{cm}^{-1}]$ and cell diameter is $d_c = 15[\mu\text{m}]$ , the intra and extracellular conductivities are $\kappa_i = 5[\text{mS} \cdot \text{cm}^{-1}]$ and $\kappa_e = 20[\text{mS} \cdot \text{cm}^{-1}]$ respectively. . . . .	55
5.11	Left the iso-potential contour in a cluster of cells after 1.0[ $\mu\text{s}$ ] of simulation. Right: the matching domain discretization used to solve the polarization process in the cell cluster. The distance between electrodes is 0.02[cm], the applied electric field is $\mathbf{E} = 5[V \cdot \text{cm}^{-1}]$ and cells diameter are $d_c = 15[\mu\text{m}]$ , the intra and extracellular conductivities are the same as for isolated cell case. . . . .	55
5.12	Circular biological cell with a transmembranic potential $V_m = -65[\text{mV}]$ at rest ( $t = 0$ ). . . . .	56
5.13	Distribution of the electric potential of the active response of a circular cell. . . . .	57
5.14	Active response of the cell to an applied electrical field of $\mathbf{E} = 10[V \cdot \text{cm}^{-1}]$ . Each curve correspond with the time curse of electric potential in a fixed angular position ( $\theta$ ) at fixed radius $r = \frac{d_c}{2}$ . . . . .	58
5.15	Response of the cell to an applied electrical field of $\mathbf{E} = 6[V \cdot \text{cm}^{-1}]$ . Each curve correspond with the time curse of electric potential in a fixed angular position on the cell interface. . . . .	59
5.16	Distribution of the electric potential of the active response of cell cluster. At top left the used non-conforming domains discretization is showed. The distance between the cells at right and left is 24 [ $\mu\text{m}$ ]. . . . .	60

5.17 Active response of a cell cluster to an applied electrical field of  $\mathbf{E} = 20[\text{V}\cdot\text{cm}^{-1}]$ .

Each curve correspond with the time course of electric potential in a fixed angular position on every cell interface. . . . . 61

## LIST OF TABLES

5.1	$h$ -convergence order for the approximation of $u_h$ and $\lambda_h$ obtained by the MFEM for matching triangular elements. . . . .	50
5.2	$h$ -convergence order for the approximation of $u_h$ and $\lambda_h$ obtained by the MFEM for non-matching triangular elements. . . . .	50

# 1 Introduction

The response of a single cell and cluster of cells to external applied electrical field is important for the understanding of techniques such as cell electroporation [1, 2], which is the transient permeabilization of the plasma membrane by means of short and intense electric pulse. This technique has broad application in the biological and medical community for instance for the local treatment of cancer. Since the cells cytosol becomes accessible to the external medium, DNA and molecules transference into the cell is possible, direct drug supply is also possible without compromising cell function [1, 2]. Moreover, it is not clear if cell electroporation does play an important role in cardiac defibrillation, therefore this is also a relevant topic in the research field of cardiac electrophysiology [3, 4, 5]. Properly studying extracellular potential distribution in cluster of cells of arbitrary geometry is important to understand the influence of applied electrical field in neurons activity [6].

Particular solutions to describe the passive response of cells to applied field are available for isolated cells of simple circular and ellipsoidal geometry [7, 8]. Although exact solutions for spherical cells in non uniform electric field exists [9, 10], a general tool to numerically investigate cells electroporation and extracellular potential distribution is of interest. In this sense, the numerical study of the passive and active response of isolated cells to external field has been made in [11, 12]. Furthermore the influence of cells arrangement, orientation and cells packing in the presence of external electrical applied field has also been investigated in [13, 14, 11, 6].

The response of biological cells to applied electrical field is a two stage process [7, 11]: the first stage takes place at the time scale of microseconds, where the capacitive current is dominant and the cell behaves like a dipole; in the second stage actual physiological changes due to the complex dynamics of ion currents on the cell membrane, which is triggered if the transmembrane current on the first stage is sufficiently high to unchain an action potential on the cell [15]. Moreover the active response of the cell will also be influenced by the distribution and packing of the cells [14, 6]. Because of the complex interactions in cells arrangements, possible irregular cells geometries and the lack of exact solutions in those cases, the study of the distribution of electric potential and of the

action potential in non-idealized systems of multiple cells can only be studied by numerical methods.

In the context of numerical methods, in particular the Finite Element Methods (FEM), simulations of cells electroporation in tumours [16], non regular cell geometry [12] and spherical cell arrangements [13] have been investigated. In [14, 6] a Hybrid Finite Element Method (HFEM) is used to investigate the passive and active cell response to external applied electrical fields. With this method the boundary value problem of electric flux conservation and the initial value problem of active cell response are decoupled and solved in alternate form in each time step. The HFEM is based on the hypothesis that cell membrane is a zero thickness domain i.e, an interface that separates two non overlapping domains [11], the intra and the extracellular domains. The membrane imposes an interface condition inside the domain which must be properly treated. In the context of finite element methods, one possible approach is to formulate separated problems in each domain and impose compatibility of the solution on the interface via Lagrange multipliers.

## 1.1 Interface problems by FEM

Proper treatment of interface conditions in finite element methods [17, 18], requires the imposition of continuity of the solution on the interface through Lagrange multipliers, as proposed by Raviart-Thomas in the known primal hybrid formulation [19]. This approach allows to have non-conforming domain discretizations with optimal convergence order for both the primal and Lagrange multiplier variables [20, 21].

In order to satisfy the compatibility condition between spaces (LBB inf-sup condition) in the primal hybrid formulation, the Lagrange multiplier must be properly defined. The formal treatment and analysis of this method are defined in the literature as Mortar Finite Element Method [20, 21, 22, 23]; and has the main advantage of allowing to solve interface problems with non-matching domain triangulations. The linear system associated with the discrete version of this formulation has a saddle point problem structure and in general is difficult to solve numerically [24]. This difficulty can be circumvent by including Galekin Least Square (GLS) stabilizations terms [25, 26, 27], or by approximating the Lagrange multiplier using a dual multiplier space. In the second case static condensation is possible for the Lagrange multiplier and effective multigrid solvers can be used [28, 22, 23].

Another form to satisfy the interface condition is to impose continuity of the primal variable and of the flux on the interface in a weak form. This gives rise to a three field domain decomposition method as proposed in [29]. Optimal order approximations for all the fields [26, 29, 30] is proved with proper stabilizations terms [25]. This method includes two Lagrange multiplier spaces, one associated with the flux on the interface and other associated to the trace of the function at the interface. The indefinite linear system obtained from the finite element discretization, is sparser and bigger than the obtained by the primal hybrid formulation due to the inclusion of two additional field to the original problem, however its advantage is the possibility of using different approximations spaces for the flux and the trace of the primal variable on the interface.

In the context of mixed finite elements [31, 32], Raviart-Thomas spaces are required [31] and continuity of the solution on the interface may be imposed by a constrained function space [32] or, in a weak form, through Lagrange multipliers. In the latter case super optimal order approximations of the primal variable may be achieved by a post-processing technique [33].

Imposing continuity of the solution on the interface through auxiliary Lagrange multipliers spaces requires the solution of an indefinite linear system. For the primal hybrid formulation this system is poorly conditioned demanding particular solution techniques [24, 28]. Another possibility to impose continuity of the solution through the interface is by penalization methods [34] or Nitsche type methods [35], where the continuity of the solution is imposed by coupled weighted terms of the primal variable defined in the interface. This family of methods generates a global system less sparse than those arising in standard conforming FEM [36]. These techniques were demonstrated to be particularly interesting to solve highly convective problems due to the inner stabilization mechanism [37].

To relax the coupling introduced by the interface terms a hybridization technique can be applied as proposed in [38] and analyzed in [39][40], which is particularly interesting when discontinuous finite elements are used in all the computational domain. In these cases a positive definite global system is assembled from local contributions by static condensation and direct linear solvers can be effectively used.



## 1.2 Objectives

In this work the active and passive response of isolated cells to applied field is investigated with a Mortar Finite Element Method MFEM. The main objective of this work is to apply the MFEM to handle the solution discontinuity due to the response of the cell interface by using non conforming domains discretizations and conforming Galerkin  $C^0$  discretizations on the rest of the domain. It is also the objective of this work to present the conditions for the existence and uniqueness to the solution of the variational formulation, the space compatibility condition and error estimate in natural norm confirmed through numerical examples. Finally, the effectiveness of the method will be demonstrated by solving the interface problem in an isolated cell and cluster of cells with non-matching discretizations.

## 1.3 Structure of the work

This work is structured as follows: in Chapter 2 the conservation law of electric flux in biological conductive mediums is presented, the interface conditions between domains of different conductivities is also introduced and an exact solution to the conservation problem for an isolated circular cell in a conductive medium is presented. In Chapter 3 a preliminary section is dedicated to the basic theory of function spaces, then the model problem is introduced and the primal hybrid variational formulation is deduced; the existence and uniqueness of the formulation is proved and the mortar finite element discretization is presented. In Chapter 4 the computational aspects of the saddle point problem are outlined. In Chapter 5 the h-convergence of the proposed method are determined and numerical results of the passive and active response of the cell are presented. Finally, in Chapter 6 the final remarks are made and the proposal for futures works are discussed.

## 2 Biological response of cell to applied electrical field

Understanding cell polarization under the action of external electrical field has wide applications in techniques as electrochemotherapy, permeabilization of cell membrane by electroporation, neuronal stimulation, cardiac pacing and cardiac defibrillation [1, 2, 6, 5]. By means of numerical simulations it is possible to understand the phenomenology of electric potential distribution in complex cell geometries and arrangements. From the conservation law of electric current in a conductive medium in the presence of a cell or a group of cells, it is possible to deduce a mathematical model based on partial differential equations (PDE) that describes the distribution of electric potential in the medium and in the biological cell.

### 2.1 Mathematical models

The electric field in a biological tissue resulting from the application of a direct current can be considered quasi-stationary [41], this means that its distribution is described by equations of the steady electric current in a volume conductor. The relation of electric current to voltage and resistance is described by Ohm's law. The electric current density  $\mathbf{J}[\text{A} \cdot \text{cm}^{-3}]$  is defined by the point form of the Ohm's law  $\mathbf{J} = \boldsymbol{\kappa} \cdot \mathbf{E}$ , where  $\mathbf{E}[\text{V} \cdot \text{cm}^{-1}]$  is the electric vector field,

$$\mathbf{E} = -\nabla u, \quad (2.1)$$

where  $u[\text{V}]$  is the scalar electric potential. In Ohm's law,  $\boldsymbol{\kappa}[\text{S} \cdot \text{cm}^{-1}]$  is the electric conductivity of the biological tissue and in the most generalized case it is a second order tensor. When conductivity is expressed in terms of a orthogonal coordinated system  $(x, y, z)$  and both the electric field and current density are related to the same coordinate system,  $\boldsymbol{\kappa}$  is diagonal with entries of the conductivity values defined on the principal directions.

By continuity of current density, the Kirchoff's law can be written in differential form as  $\text{div}(\mathbf{J}) = \rho_s$ , where  $\rho_s[\text{A} \cdot \text{cm}^{-3}]$  is an applied source current. Now by Ohm's law applied

to a electric field, we can write Kirchoff's law in terms of the electric potential  $u$  as,

$$-\operatorname{div}(\boldsymbol{\kappa}\nabla u) = \rho_s, \quad (2.2)$$

which is known as the Poisson's equation that describe the electric potential distribution in a resistive biological tissue with an applied source current. The boundary value problem (2.2) requires additional conditions in order to be well posed. Dirichlet boundary conditions can be defined on the domain's boundary to denote an applied voltage, or Neumann boundary conditions when a current source is applied on some portion of the boundary.

Now it is possible to formally present the boundary value problem defined on a domain  $\Omega \subset \mathbb{R}^d$ , where  $d \in \{1, 2, 3\}$  with a Lipschitz boundary  $\partial\Omega = \Gamma_D \cup \Gamma_N, \Gamma_D \cap \Gamma_N = \emptyset$ , that describe the electric potential distribution in a conductive biological tissue or cell in the presence of an applied current  $\rho_s$ :

$$\begin{aligned} -\operatorname{div}(\boldsymbol{\kappa}\nabla u) &= \rho_s(\mathbf{x}), \quad \text{in } \Omega \\ u &= \hat{u}, \quad \text{on } \Gamma_D \\ \nabla u \cdot \mathbf{n} &= \rho_n, \quad \text{on } \Gamma_N \end{aligned} \quad (2.3)$$

Where  $\hat{u}$  is the known scalar electric potential defined on the Dirichlet boundary portion  $\Gamma_D$ , and  $\rho_n$  is the applied current on the Neumann boundary portion of the domain  $\Gamma_N$ .

### 2.1.1 Model for electric response of a cell

Based on the law of charge conservation, we describe the problem of electric potential distribution on a system with a conductive circular cell in a conductive medium subject to an applied electric field  $\mathbf{E}$  as depicted in Figure 2.1,

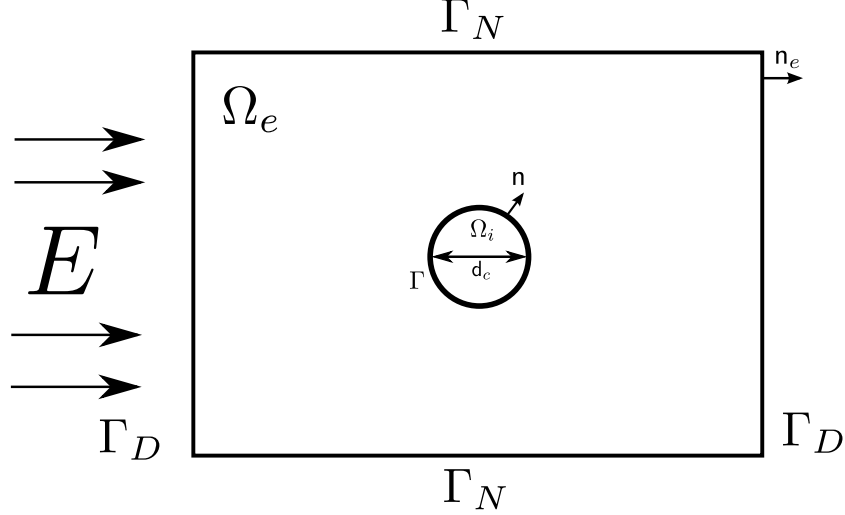


Figure 2.1: A circular cell in a conductive medium

The cell diameter is denoted as  $d_c$  and the electric conductivity of the cell is  $\kappa_i$ . The bounded domain  $\Omega_e$  with electrical conductivity  $\kappa_e$  is subject to an applied electric field  $\mathbf{E}$  as depicted in Figure 2.1. The Poisson's equation of charge conservation (2.4) for the proposed system is written as a function of the electric potential inside ( $u_i$ ) and outside ( $u_e$ ) the cell:

$$\begin{aligned}
 -\operatorname{div}(\kappa_e \nabla u_e) &= 0, & \text{in } \Omega_e, \\
 -\operatorname{div}(\kappa_i \nabla u_i) &= 0, & \text{in } \Omega_i, \\
 -\kappa_i \nabla u_i \cdot \mathbf{n} &= -\kappa_e \nabla u_e \cdot \mathbf{n} = I_m, & \text{on } \Gamma, \\
 u_e &= \hat{u}, & \text{on } \Gamma_D, \\
 \nabla u_e \cdot \mathbf{n}_e &= 0, & \text{on } \Gamma_N.
 \end{aligned} \tag{2.4}$$

In this work we limit to two dimensional problems, under the hypothesis that the cell membrane is a zero thickness domain with a characteristic membrane resistance  $R_m$  measured in  $[\text{k} \cdot \Omega \text{cm}^2]$  and characteristic capacitance  $C_m$  per unit area measured in  $[\mu\text{F} \cdot \text{cm}^{-2}]$ .

The supplementary interface condition defined on  $\Gamma$  in problem (2.4) implies continuity

of the transmembrane current,

$$-\boldsymbol{\kappa}_i \nabla u_i \cdot \mathbf{n} = -\boldsymbol{\kappa}_e \nabla u_e \cdot \mathbf{n} = I_m, \quad \text{on } \Gamma,$$

where  $\Gamma$  is the membrane of the circular cell,  $\mathbf{n}$  is the unitary normal vector pointing outside of  $\Gamma$  and  $I_m [\text{A} \cdot \text{cm}^{-2}]$  is the transmembrane current which has two components: a capacitive and a resistive current, both depending on the transmembrane potential defined by,

$$V_m = u_i - u_e, \quad \text{on } \Gamma. \quad (2.5)$$

The transmembrane current can be written as the contribution of two currents: the capacitive and the resistive or ionic current given by,

$$I_m = C_m \frac{\partial V_m}{\partial t} + I_{ion}(V_m, \mathbf{q}), \quad \text{on } \Gamma. \quad (2.6)$$

The capacitive current is a consequence of the electric isolation property of the cell membrane. The cell polarization due to capacitive currents occurs at the time scale of microseconds, whereas for the active response of the cell membrane, the resistive or ionic current acts at time scale of milliseconds and is determined by the complex dynamics of the Sodium, Potassium and leakage ionic currents, described by the non-linear equations of the Hodgkin-Huxley model [42, 15] represented by the state variable  $\mathbf{q}$  in equation (2.6).

Under certain conditions the system of equations (2.4) describing cell polarization of an isolated circular cell may be solved using dimensional analysis and leading order arguments as in [7] or using Legendre functions and symbolic computational tools for a spherical cell as in [10]. Exact solutions have shown to have a good correlation with experimental results as reported in [9, 10, 12]. Here is presented an expression for the exact solution for the intra and extracellular electric potential problem (2.4) in a polar system  $(r, \theta)$  as shown in Figure 2.2, this solution assume the additional hypothesis that the passive ionic current is purely resistive  $I_{ion}(V_m, q) = \frac{V_m}{R_m}$  and that the cell transmembrane potential at rest is  $V_m = 0$ , see [11, 7].

The exact solution is given by:

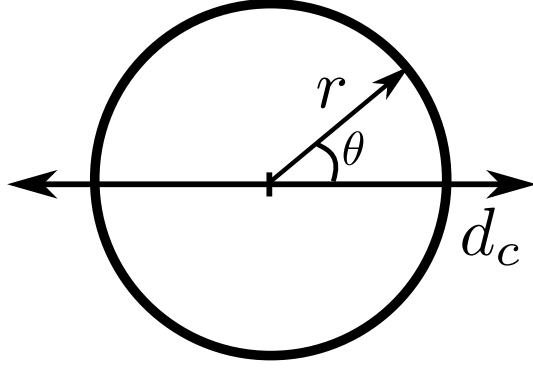


Figure 2.2: Polar reference system used in the exact solution.

$$\begin{aligned}
 u_i(r, \theta, t) &= -a(t) \cdot E r \cos(\theta), \quad r < \frac{d_c}{2} \\
 u_e(r, \theta, t) &= -E r \cos(\theta) - b(t) \cdot E \frac{d_c^2}{4r} \cos(\theta), \quad r > \frac{d_c}{2} \\
 V_m(\theta, t) &= E d_c \cos(\theta) (1 - e^{-t/\tau_{ip}}) (1 - \epsilon).
 \end{aligned} \tag{2.7}$$

Where

$$\begin{aligned}
 a(t) &= \frac{2\kappa_e}{\kappa_i + \kappa_e} \left\{ e^{-t/\tau_{ip}} + \epsilon (1 - e^{-t/\tau_{ip}}) \right\} \\
 b(t) &= 1 - \frac{2\kappa_i}{\kappa_i + \kappa_e} \left\{ e^{-t/\tau_{ip}} + \epsilon (1 - e^{-t/\tau_{ip}}) \right\} \\
 \tau_{ip} &= \left\{ \frac{1}{C_m R_m} + \frac{2\kappa_i \kappa_e}{C_m d_c (\kappa_i + \kappa_e)} \right\} \\
 \epsilon &= \frac{\tau_{ip}}{C_m R_m}
 \end{aligned}$$

The passive response of the cell take place at the characteristic time scale  $\tau_{ip}$  of microseconds. In Chapter 5 the phenomenology of cell polarization described by this solution is presented. Even though exact solutions as (2.7) exists to describe the passive response of the cell in simple geometries, it is a limited tool to solve more general cases. In the next chapter, the variational formulation of the conservation problem (2.4) is presented, this approach will be the ground base to find approximated solutions of general cases problems.

### 2.1.2 The Hodgkin-Huxley model

In 1952 Alan Lloyd Hodgkin and Andrew Fielding Huxley determined in a quantitative form [42] the relation between the main ionic currents going through the cell membrane

and the transmembrane potential describing the propagation of action potential on the giant squid axon. The main ionic currents described by the Hodgkin-Huxley HH model are the sodium, potassium and leakage current  $I_{Na}$ ,  $I_K$ ,  $I_l$  respectively. The HH model idealize the flux of electric current through the cell membrane as a closed circuit between the intra and extracellular domain, the transmembrane potential in the absence of an applied current is given by the balance between the capacitive and ionic currents:

$$-C_m \frac{dV_m}{dt} = I_{Na} + I_K + I_l, \quad (2.8)$$

where  $C_m$  is the electric capacitance of the lipid bilayer of the cell membrane measured in  $[\mu\text{F} \cdot \text{cm}^2]$ . Each ionic currents can be expressed as function of the ionic conductivity of the sodium, potassium and others ( $g_{Na}$ ,  $g_K$ ,  $g_l$ ) as:

$$I_{Na} = g_{Na}(V_m - E_{Na}), \quad (2.9)$$

$$I_K = g_K(V_m - E_K), \quad (2.10)$$

$$I_l = g_l(V_m - E_l), \quad (2.11)$$

where  $E_{Na}$ ,  $E_K$  and  $E_l$  are the potential of equilibrium for each species. The great contribution of the HH model was the description of the ionic conductivities ( $g_{Na}$ ,  $g_K$ ,  $g_l$ ) during the action potential in function of the transmembrane potential  $V_m$ . The ionic conductivity of sodium and potassium are given by:

$$g_{Na} = \bar{g}_{Na} m^3 h, \quad (2.12)$$

$$\frac{dm}{dt} = \alpha_m(1 - m) - \beta_m m, \quad (2.13)$$

$$\frac{dh}{dt} = \alpha_h(1 - h) - \beta_h h, \quad (2.14)$$

$$g_K = \bar{g}_K n^4, \quad (2.15)$$

$$\frac{dn}{dt} = \alpha_n(1 - n) - \beta_n n, \quad (2.16)$$

where  $\bar{g}_{Na}$  and  $\bar{g}_K$  are the maximal conductance value measured in  $[\text{S} \cdot \text{cm}^{-2}]$  of the sodium and potassium,  $m$ ,  $h$  and  $n$  are dimensionless variables  $\in [0, 1]$  related to the activation of the sodium and potassium ion channels;  $\alpha_m$ ,  $\alpha_h$ ,  $\beta_m$ ,  $\beta_h$ ,  $\alpha_n$  and  $\beta_n$  are functions of  $V_m$

and represent the activation and deactivation rate of the associated ion channels:

$$\alpha_m = \frac{0.1(V_m + 25)}{e^{\frac{V_m+25}{10}} - 1}, \quad (2.17)$$

$$\beta_m = 4e^{\frac{V_m}{18}}, \quad (2.18)$$

$$\alpha_h = 0.07e^{\frac{V_m}{20}}, \quad (2.19)$$

$$\beta_h = \frac{1}{e^{\frac{V_m+30}{10}} + 1}, \quad (2.20)$$

$$\alpha_n = \frac{0.01(V_m + 10)}{e^{\frac{V_m+10}{10}} - 1}, \quad (2.21)$$

$$\beta_n = 0.125e^{\frac{V_m}{80}}. \quad (2.22)$$

The electric conductivity associated to the leakage ionic current  $g_l$  is simply determined as  $g_l = \bar{g}_l$  the maximal conductance value. The final expression of the HH model is then:

$$-C_m \frac{dV_m}{dt} = \bar{g}_{Na} m^3 h (V_m - E_{Na}) + \bar{g}_K n^4 (V_m - E_K) + \bar{g}_l (V_m - E_l) - I_m, \quad (2.23)$$

where  $I_m$  is the transmembrane current, in this work the transmembrane current on the active response of the cell, will be considered to be the applied current due to an electric field that will trigger or not the action potential on the cell membrane. For a detailed description over the experimental setting and the physiological considerations see [15, 42].

In Figure 2.3 the transmembrane potential  $V_m$  describing the action potential typical of the giant squid axon described by the HH model is plotted, the activations variables of the model  $m, n$  and  $h$  are also shown. The parameters to reproduce the action potential are:  $\bar{g}_{Na} = 120[\text{mS} \cdot \text{cm}^{-2}]$ ,  $\bar{g}_K = 36[\text{mS} \cdot \text{cm}^{-2}]$ ,  $\bar{g}_l = 0.3[\text{mS} \cdot \text{cm}^{-2}]$ ,  $E_{Na} = 115[\text{mV}]$ ,  $E_K = -12[\text{mV}]$ ,  $E_l = 10.6[\text{mV}]$ ,  $C_m = 1[\mu\text{F} \cdot \text{cm}^{-2}]$ ,  $I_m = 5[\mu\text{A} \cdot \text{cm}^{-2}]$  and  $(m, n, h) = (0.1, 0.33, 0.6)$  at  $t = 0$ . The transmembrane potential  $V_m$  is considered to be a deviation from the equilibrium state of the cell  $V_m = V - V_{eq}$  where the typical value of  $V_{eq}$  for the experimental setting of the HH model is  $V_{eq} = -65[\text{mV}]$ , see [15, 42].



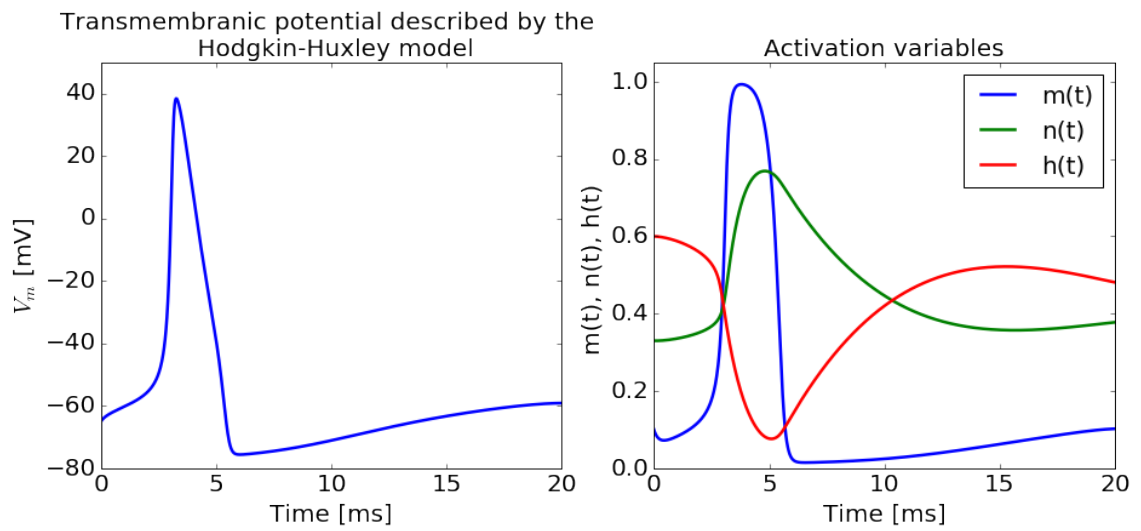


Figure 2.3: Transmembrane potential following the action potential described the Hodgkin-Huxley model for an applied current  $I_m = 5[\mu\text{A} \cdot \text{cm}^{-2}]$  and activation variables of the ions channels.

# 3 The Mortar Finite Element Method

In this chapter the notation used in this work is introduced and some aspects of the functional space where the mortar finite element method is based are also presented. The variational formulation of the second order interface problem of the cell response to applied electric field is introduced and, the conditions for the existence and uniqueness of the solution as proposed by Raviart-Thomas [19] are presented, finally the a priori error estimative of the discrete problem is briefly presented.

## 3.1 Preliminaries

The adopted notation in this work is the following,  $u$ ,  $v$  and  $\phi$  denote scalar fields;  $\mathbf{u}$ ,  $\mathbf{v}$ ,  $\boldsymbol{\phi}$  denote vectorial fields. We consider a bounded domain  $\Omega \subset \mathbb{R}^2$ , with a Lipschitz boundary  $\partial\Omega$  and bounded real valued functions  $f \in L^2(\Omega)$ , where  $L^2(\Omega)$  denotes the space of functions square integrable in  $\Omega$ .

For a given  $m \geq 0 \in \mathbb{N}$ , we denote the Hilbert space  $H^m(\Omega)$  of order  $m$  on  $\Omega$  containing functions  $v \in L^2(\Omega)$  such that the  $m$ -th derivative in the sense of distributions are defined in  $L^2(\Omega)$ , that is:

$$H^m = \{v \in L^2(\Omega); D^\alpha v \in L^2(\Omega), |\alpha| \leq m\}, \quad \text{where,} \quad (3.1)$$

$$D^\alpha(\cdot) = \frac{\partial^\alpha(\cdot)}{\partial x_1^{\alpha_1} \partial x_2^{\alpha_2}}, \quad |\alpha| = \alpha_1 + \alpha_2, \quad (3.2)$$

and  $\alpha$  is a vector of non-negative integer entries. The inner product defined in  $H^m(\Omega)$  and its associated norm are given by:

$$(v, w)_m := \sum_{|\alpha| < m} \int_{\Omega} D^\alpha v D^\alpha w dx, \quad \|v\|_m^2 = (v, v)_m. \quad (3.3)$$

The space  $L^2(\Omega)$  is then  $H^0(\Omega)$  and in this work the associated norm  $\|v\|_{L^2(\Omega)}$  will simply be denoted by  $\|v\|_0$ .

The particular Hilbert spaces of interest in the present work are:  $L^2(\Omega)$ ,  $H^1(\Omega)$ ,  $H_0^1(\Omega)$  and  $H^{\frac{1}{2}}(\Omega)$ . If the boundary of the bounded domain  $\Omega$ , denoted by  $\partial\Omega$  is a Lipschitz continuous domain, there exists a linear and continuous operator  $\gamma_0 : H^1(\Omega) \rightarrow L^2(\partial\Omega)$  called the trace operator;  $\gamma_0$  applied to  $v \in H^1(\Omega)$  is simply the restriction of  $v$  to  $\partial\Omega$ , denoted as  $v|_{\partial\Omega}$ . The application of the trace operator  $\gamma_0$  to  $H^1(\Omega)$ ,  $\gamma_0(H^1(\Omega))$  belongs to a family of normed Hilbert spaces  $H^s(\partial\Omega)$  with  $s \in \mathbb{R}$ , in particular:

$$\gamma_0(H^1(\Omega)) := H^{\frac{1}{2}}(\partial\Omega),$$

with the associated norm,

$$\|\gamma_0 v\|_{H^{\frac{1}{2}}(\partial\Omega)} := \inf_{v \in H^1(\Omega)} \|v\|_{H^1(\Omega)}.$$

The dual space of  $H^{\frac{1}{2}}(\partial\Omega)$  is denoted by  $H^{-\frac{1}{2}}(\partial\Omega)$ , and the duality relation between these two spaces is given by,

$$\langle \cdot, \cdot \rangle_{\partial\Omega} := \int_{\partial\Omega} \mu v ds.$$

### ***3.1.1 Linear variational formulation problems of one field***

The linear variational problem of a single field can be represented in an abstract form as, given  $f \in \mathcal{U}'$  find  $u \in \mathcal{U}$  such that:

$$a(u, v) = f(v), \quad \forall v \in \mathcal{U}, \quad (3.4)$$

where  $\mathcal{U}$  is a Hilbert space,  $\mathcal{U}'$  the associated dual space and  $a(\cdot, \cdot) : \mathcal{U} \times \mathcal{U} \rightarrow \mathbb{R}$  is a bilinear form. For cases where the bilinear form is symmetric and positive definite, this problem is equivalent to the following minimization problem: find  $u \in \mathcal{U}$  such that

$$J(u) \leq J(v), \quad \forall v \in \mathcal{U},$$

with

$$J(v) = \frac{1}{2}a(v, v) - f(v), \quad \forall v \in \mathcal{U}.$$

The analysis of the existence and uniqueness to the solution of problem (3.4) is ensured by the Lax-Milgram theorem.

**Theorem 3.1. (The Lax-Milgram theorem).** *If  $\mathcal{U}$  is a Hilbert space,  $f : \mathcal{U} \rightarrow \mathbb{R}$  a continuous linear functional and  $a(\cdot, \cdot) : \mathcal{U} \times \mathcal{U} \rightarrow \mathbb{R}$  is a bilinear form such that:*

1. *It is continuous: there exists a constant  $0 < M < \infty$  such that*

$$|a(u, v)| \leq M \|u\|_{\mathcal{U}} \|v\|_{\mathcal{U}} \quad \forall u, v \in \mathcal{U} \quad (3.5)$$

2. *It is  $\mathcal{U}$ -Elliptic: there exists a constant  $\alpha > 0$  such that*

$$|a(u, v)| \geq \alpha \|u\| \|v\| \quad \forall u, v \in \mathcal{U} \quad (3.6)$$

*then the variational problem (3.4) has a unique solution.*

### 3.1.2 Linear mixed variational formulation problems

Linear variational problems on the presence of internal constrains handled via Lagrange multipliers [19], leads to variational problems of two fields commonly denoted as mixed problems [32]; postulated here in abstract form as, given  $f \in \mathcal{U}'$  and  $g \in \mathcal{M}'$ , find  $(u, \lambda) \in \mathcal{U} \times \mathcal{M}$  such that:

$$\begin{aligned} a(u, v) + b(v, \lambda) &= f(v), \quad \forall v \in \mathcal{U}, \\ b(u, \mu) &= g(\mu), \quad \forall \mu \in \mathcal{M}, \end{aligned} \quad (3.7)$$

where  $\mathcal{U}$  and  $\mathcal{M}$  are Hilbert spaces,  $a : \mathcal{U} \times \mathcal{U} \rightarrow \mathbb{R}$ ,  $b : \mathcal{U} \times \mathcal{M} \rightarrow \mathbb{R}$  are continuous bilinear forms and  $f : \mathcal{U} \rightarrow \mathbb{R}$  and  $g : \mathcal{M} \rightarrow \mathbb{R}$  are continuous linear functionals. The bilinear forms  $a(\cdot, \cdot)$  and  $b(\cdot, \cdot)$  defines the following norms:

$$\begin{aligned} \|a\| &= \sup_{u, v \in \mathcal{U}} \frac{a(u, v)}{\|u\|_{\mathcal{U}} \|v\|_{\mathcal{U}}}, \\ \|b\| &= \sup_{v \in \mathcal{U}, \mu \in \mathcal{M}} \frac{b(v, \mu)}{\|v\|_{\mathcal{U}} \|\mu\|_{\mathcal{M}}}, \end{aligned}$$

and also defines the following linear continuous operators  $A : \mathcal{U} \rightarrow \mathcal{U}'$ ,  $B : \mathcal{U} \rightarrow \mathcal{M}'$  and  $B^t : \mathcal{M} \rightarrow \mathcal{U}'$  given by:

$$\langle Au, v \rangle_{\mathcal{U}' \times \mathcal{U}} = a(u, v), \quad \forall u, v \in \mathcal{U},$$

$$\langle Bv, \mu \rangle_{\mathcal{M}' \times \mathcal{M}} = \langle v, B^T \mu \rangle_{\mathcal{U} \times \mathcal{U}'}, \quad \forall v \in \mathcal{U}, \quad \mu \in \mathcal{M}.$$

When the bilinear form  $a(\cdot, \cdot)$  is symmetric and elliptic in the space:

$$K(0) = \{v \in \mathcal{U}; b(v, \mu) = 0, \quad \forall \mu \in \mathcal{M}\}, \quad (3.8)$$

it is possible to associated problem (3.7) with the following minimization problem, find  $u \in K(g)$  such that:

$$J(v) = \frac{1}{2}a(v, v) - f(v), \quad \text{in } K(g),$$

with

$$K(g) = \{v \in \mathcal{U}; b(v, \mu) = g(\mu), \quad \forall \mu \in \mathcal{M}\}.$$

Using the technique of Lagrange multiplier, the problem (3.7) can be transformed in the following saddle point problem, find  $(u, \lambda) \in \mathcal{U} \times \mathcal{M}$  such that:

$$L(u, \mu) \leq L(u, \lambda) \leq L(v, \lambda), \quad \forall v \in \mathcal{U}, \quad \forall \mu \in \mathcal{M} \quad (3.9)$$

where  $L(v, \mu)$  is the Langrangian functional,

$$L(v, \lambda) = J(v) + (Bv - g, \lambda) \quad (3.10)$$

with  $\lambda$  the Lagrange multiplier.

The conditions for the existence and uniqueness of the problem (3.7) is presented here through the auxiliary problem: find  $u \in K(g)$  such that

$$a(u, v) = f(v), \quad \forall v \in \ker(B) = K(0). \quad (3.11)$$

Note that if  $(u, \lambda) \in \mathcal{U} \times \mathcal{M}$  solves problem (3.7), then  $u \in K(g)$  also solves problem (3.11). Now, the conditions to satisfy the inverse relation, this is, given  $u \in K(g)$  solving problem (3.11) there exist a pair  $(u, \lambda) \in \mathcal{U} \times \mathcal{M}$  solving problem (3.7) are given in the following theorem.

**Theorem 3.2. (Brezzi theorem).** *If  $\mathcal{U}$  and  $\mathcal{M}$  are Hilbert spaces,  $f : \mathcal{U} \rightarrow \mathbb{R}$  and  $g : \mathcal{M} \rightarrow \mathbb{R}$  are continuous linear functionals and  $a(\cdot, \cdot) : \mathcal{U} \times \mathcal{U} \rightarrow \mathbb{R}$  and  $b(\cdot, \cdot) : \mathcal{U} \times \mathcal{M} \rightarrow \mathbb{R}$  are bilinear forms which satisfied:*

1. *Continuity: there exists two constants  $0 < M_1, M_2 < \infty$  such that*

$$|a(u, v)| \leq M_1 \|u\|_{\mathcal{U}} \|v\|_{\mathcal{U}} \quad \forall u, v \in \mathcal{U}$$

$$|b(u, \lambda)| \leq M_2 \|u\|_{\mathcal{U}} \|\lambda\|_{\mathcal{M}} \quad \forall u \in \mathcal{U} \quad \forall \lambda \in \mathcal{M}$$

2. *K-Coercivity of a: exists two constants  $\alpha_1 > 0$  and  $\alpha_2 > 0$  such that*

$$\sup_{v \in K} \frac{|a(u, v)|}{\|v\|_{\mathcal{U}}} \geq \alpha_1 \|u\|_{\mathcal{U}} \quad \forall u \in K$$

$$\sup_{u \in K} \frac{|a(u, v)|}{\|u\|_{\mathcal{U}}} \geq \alpha_2 \|v\|_{\mathcal{U}} \quad \forall v \in K$$

where,

$$K(0) = \{u \in \mathcal{U}; b(u, \mu) = 0 \quad \forall \mu \in \mathcal{M}\}$$

3. *LBB-condition: exists a constant  $\beta > 0$  such that*

$$\sup_{v \in \mathcal{U}} \frac{|b(v, \lambda)|}{\|v\|_{\mathcal{U}}} \geq \beta \|\lambda\|_{\mathcal{M}} \quad \forall \lambda \in \mathcal{M}$$

*Then the problem (3.7) has a unique solution.*

After this short presentation of the basic theory of variational problems, the variational formulation and finite element discretization for the model problem of the response of a cell to an applied electric field, is introduced and briefly analysed.

## 3.2 The model problem

Recalling that the conservation problem of electric current of the unicellular system in Figure 3.1, is given by equation (3.12).

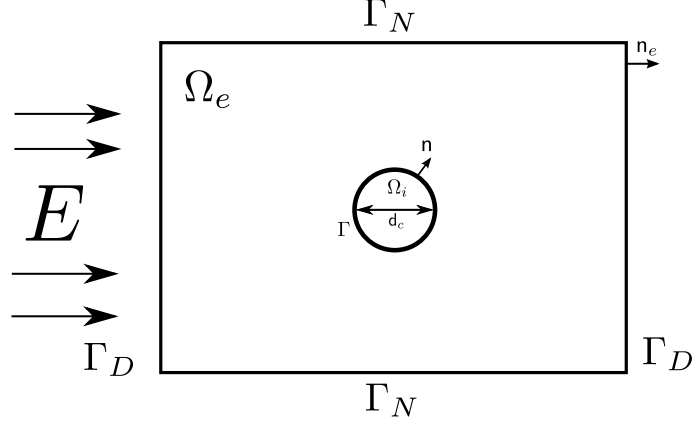


Figure 3.1: A circular cell in a conductive medium

$$\begin{aligned}
 -\operatorname{div}(\boldsymbol{\kappa}_e \nabla u_e) &= 0, & \text{in } \Omega_e, \\
 -\operatorname{div}(\boldsymbol{\kappa}_i \nabla u_i) &= 0, & \text{in } \Omega_i, \\
 -\boldsymbol{\kappa}_i \nabla u_i \cdot \mathbf{n} &= -\boldsymbol{\kappa}_e \nabla u_e \cdot \mathbf{n} = I_m, & \text{on } \Gamma, \\
 u_i - u_e &= V_m, & \text{on } \Gamma, \\
 u_e &= \hat{u}, & \text{on } \Gamma_D, \\
 \nabla u_e \cdot \mathbf{n}_e &= 0, & \text{on } \Gamma_N.
 \end{aligned} \tag{3.12}$$

Now let  $\boldsymbol{\kappa}_i = \boldsymbol{\kappa}_e$  to be equal electric conductivity inside and outside the cell. It is possible to rewrite the system (3.12) including  $\hat{u}$  the electric potential applied on  $\Gamma_D$  as,

$$\begin{aligned}
 -\Delta u_e &= 0, & \text{in } \Omega_e, \\
 -\Delta u_i &= 0, & \text{in } \Omega_i, \\
 -\nabla u_i \cdot \mathbf{n} &= -\nabla u_e \cdot \mathbf{n} = I_m, & \text{on } \Gamma, \\
 u_i - u_e &= V_m, & \text{on } \Gamma, \\
 u_e &= \hat{u}, & \text{on } \Gamma_D, \\
 \nabla u_e \cdot \mathbf{n}_e &= 0, & \text{on } \Gamma_N.
 \end{aligned} \tag{3.13}$$

The variational formulation of problem (3.13), is written to reduce the required

regularity of the candidate solution as: find  $u \in \mathcal{U}$  such that,

$$\int_{\Omega} -\Delta u v dx = 0, \quad \forall v \in \mathcal{V} \quad (3.14)$$

where  $\Omega = \Omega_i \cup \Omega_e$ ,  $\Gamma = \Omega_i \cap \Omega_e$ ,  $u = (u_i, u_e)$ ,  $v = (v_i, v_e)$ . Using Green's identity we can rewrite (3.14) as,

$$\int_{\Omega} \nabla u \cdot \nabla v dx - \int_{\partial\Omega \setminus \Gamma} \nabla u \cdot \mathbf{n}_e v ds = 0, \quad \forall v \in \mathcal{V} \quad (3.15)$$

where the space of candidate solutions  $\mathcal{U}$  and the associated space of variations  $\mathcal{V}$  are:

$$\mathcal{U} = \left\{ u \in L^2(\Omega), (u_i, u_e) \in (H^1 \times H^1) : u_i|_{\Gamma} - u_e|_{\Gamma} = V_m, u_e|_{\Gamma_D} = \hat{u} \right\}; \quad (3.16)$$

$$\mathcal{V} = \left\{ v \in L^2(\Omega), (v_i, v_e) \in (H^1 \times H^1) : v_i|_{\Gamma} - v_e|_{\Gamma} = 0, v_e|_{\Gamma_D} = 0 \right\} \quad (3.17)$$

and the associated unconstrained product spaces are given by:

$$\tilde{\mathcal{U}} = \left\{ u \in L^2(\Omega), (u_i, u_e) \in (H^1 \times H^1), u_e|_{\Gamma_D} = \hat{u} \right\}; \quad (3.18)$$

$$\tilde{\mathcal{V}} = \left\{ v \in L^2(\Omega), (v_i, v_e) \in (H^1 \times H^1), v_e|_{\Gamma_D} = 0 \right\}. \quad (3.19)$$

A short type expression for the constrained interface condition  $v_i|_{\Gamma} - v_e|_{\Gamma} = 0$  and  $u_i|_{\Gamma} - u_e|_{\Gamma} = V_m$ , is the scalar Jump  $[\cdot]$  of  $(v, u)$  on  $\Gamma$ , defined as  $v_i|_{\Gamma} - v_e|_{\Gamma} = [v] = 0$  and  $[u] = V_m$ . Now, as proposed by Raviart-Thomas [19], an additional Hilbert space defined on  $\Gamma$  is included to impose the interface condition of the primal variable, i.e  $[u] = V_m$  or equivalently  $[u] - V_m = 0$  on  $\Gamma$  in a weak form employing a Lagrange multiplier. With this technique the constraint over  $v$  ( $[v] = 0$  on  $\Gamma$ ) on the space  $\mathcal{V}$  is also relaxed and thus the primal hybrid variational formulation is: find  $(u, \lambda) \in (\tilde{\mathcal{U}} \times \mathcal{M})$  such that,

$$\begin{aligned} \int_{\Omega} \nabla u \cdot \nabla v dx - \int_{\partial\Omega \setminus \Gamma} \nabla u \cdot \mathbf{n}_e v ds + \int_{\Gamma} \mu([u] - V_m) ds \\ + \int_{\Gamma} \lambda[v] ds = 0, \quad \forall (v, \mu) \in \tilde{\mathcal{V}} \times \mathcal{M}, \end{aligned} \quad (3.20)$$

where  $\lambda$  is the Lagrange multiplier and  $\mu$  is the admissible variation related to  $\mathcal{M}$ , which is the Hilbert space of the Lagrange multiplier. By duality argument, we note that  $\mathcal{M} =$



$H^{-\frac{1}{2}}(\Gamma)$ , which is the dual space of  $H^{\frac{1}{2}}(\Gamma)$  and therefore  $\mu \in H^{-\frac{1}{2}}(\Gamma)$ . The variational formulation (3.20) can be derived from a minimization problem under a relaxed manifold and is known as a saddle point problem, see [19, 32]. By the natural Neumann boundary condition in (3.13)(f)  $\nabla u \cdot \mathbf{n}_e = 0$  on  $\Gamma_N$ , the second term of the formulation is neglected, and then the saddle point problem is: find  $(u, \lambda) \in (\tilde{\mathcal{U}}, \mathcal{M})$  such that

$$a(u, v) + b(v, \lambda) = 0, \quad \forall v \in \tilde{\mathcal{V}} \quad (3.21)$$

$$b(u, \mu) = g(\mu), \quad \forall \mu \in \mathcal{M}$$

with  $a(u, v) = \int_{\Omega} \nabla u \cdot \nabla v dx$ ,  $b(v, \mu) = \int_{\Gamma} \mu[v] ds$  and  $g(\mu) = \int_{\Gamma} \mu V_m ds$ . A different way to write a variational formulation of the original interface problem (3.13) is now presented. The objective is to find the relation between the interface condition of flux conservation on (3.13)(c) and how this is satisfied by the formulation (3.21). Assuming that we chose two functions  $(v_i, v_e) \in \tilde{\mathcal{V}}$  with compact support on  $(\Omega_i, \Omega_e)$  respectively, multiplying by the two first equations in (3.13) and using the Green's integration identity, the following variational problem is obtained: find  $(u_i, u_e) \in \tilde{\mathcal{U}}$  such that

$$\begin{aligned} \int_{\Omega_e} \nabla u_e \cdot \nabla v_e dx - \int_{\partial\Omega \setminus \Gamma} \nabla u_e \cdot \mathbf{n}_e v_e ds + \int_{\Gamma} \nabla u_e \cdot \mathbf{n} v_e ds &= 0, \quad \forall v \in \tilde{\mathcal{V}}, \\ \int_{\Omega_i} \nabla u_i \cdot \nabla v_i dx - \int_{\Gamma} \nabla u_i \cdot \mathbf{n} v_i ds &= 0, \quad \forall v \in \tilde{\mathcal{V}}, \end{aligned} \quad (3.22)$$

where  $(u_i, u_e)$  must satisfy the interface conditions  $[u] = V_m$  on  $\Gamma$  and  $-\nabla u_i \cdot \mathbf{n} = -\nabla u_e \cdot \mathbf{n} = I_m$ , on  $\Gamma$  with  $\mathbf{n} = \mathbf{n}_i = -\mathbf{n}_e$  the normal unitary vector pointing outward  $\Gamma$ . Considering that the flux interface condition is explicitly written in (3.22) and that the Neumann boundary condition of 3.13(f) on  $\Gamma_N$  is included on the formulation, it is possible to rewrite (3.22) as:

$$\begin{aligned} \int_{\Omega_e} \nabla u_e \cdot \nabla v_e dx - \int_{\Gamma} I_m v_e ds &= 0, \quad \forall v \in \tilde{\mathcal{V}}, \\ \int_{\Omega_i} \nabla u_i \cdot \nabla v_i dx + \int_{\Gamma} I_m v_i ds &= 0, \quad \forall v \in \tilde{\mathcal{V}}, \end{aligned} \quad (3.23)$$

As postulated  $(v_i, v_e)$  have compact support on  $(\Omega_i, \Omega_e)$ , therefore it is possible to define a unique function  $u = (u_i, u_e)$  and  $v = (v_i, v_e)$  such that by adding the two first

equations on (3.23) we have the equivalent variational formulation: find  $u \in \tilde{\mathcal{U}}$  such that

$$\int_{\Omega} \nabla u \cdot \nabla v dx + \int_{\Gamma} I_m[v] ds = 0, \quad \forall v \in \tilde{\mathcal{V}}, \quad (3.24)$$

Choosing  $I_m := \lambda$  i.e the transmembrane current to be the Lagrange multiplier defined on  $\Gamma$  and by including the interface condition  $[u] = V_m$  on  $\Gamma$  in a weak form with the function of admissible variations of  $\lambda \in \mathcal{M}$ , this is  $\mu \in \mathcal{M}$ , equation (3.24) recovers the primal hybrid variational formulation (3.21): find  $(u, \lambda) \in (\tilde{\mathcal{U}}, \mathcal{M})$  such that

$$\begin{aligned} \int_{\Omega} \nabla u \cdot \nabla v dx + \int_{\Gamma} \lambda[v] ds &= 0, \quad \forall v \in \tilde{\mathcal{V}}, \\ \int_{\Gamma} \mu[u] ds &= \int_{\Gamma} \mu V_m ds, \quad \forall \mu \in \mathcal{M}, \end{aligned} \quad (3.25)$$

In this process the following relation can be identified,  $I_m \equiv \lambda \equiv -\nabla u_i \cdot \mathbf{n} \equiv -\nabla u_e \cdot \mathbf{n}$ .

### 3.2.1 Existence and uniqueness of the saddle point problem

The essential points to proof the existence and uniqueness of the solution to the saddle point problem (3.25) are: continuity, coercivity and suitable inf-sup condition. The proof for the general interface problem (3.25) is fully detailed in [23], however here for the sake of presentation the proof will be presented as in [19, 21], where the interface condition over  $\Gamma$  of the primal variable is simply:  $[u] = V_m = 0$  and the general Dirichlet condition  $u_e|_{\Gamma_D} = \hat{u}$  is replaced by the homogeneous condition in all the boundary, that is  $u_e|_{\partial\Omega} = 0$  with  $\partial\Omega = \Gamma_D \cup \Gamma_N$ .

The Hilbert space  $H_0^1(\Omega)$  can be defined as a subspace of  $\tilde{\mathcal{V}}$  containing the functions satisfying the matching condition over the interface in a weak form, that is,

$$(v, \mu) \rightarrow b(v, \mu) = \int_{\Gamma} [v] \mu ds = 0, \quad \forall \mu \in \mathcal{M}. \quad (3.26)$$

Using the Hahn-Banach theorem as presented by Raviart and Thomas in [19], it can be proved that a Hilbert space  $\mathcal{H}$  with the same characteristics of  $H_0^1(\Omega)$  can be defined as:

$$\mathcal{H} := \left\{ v \in \tilde{\mathcal{V}}, \quad b(v, \mu) = 0, \quad \forall \mu \in \mathcal{M}(\Gamma) \right\}.$$

Now let  $(u, \lambda) \in (\tilde{\mathcal{V}} \times \mathcal{M})$  be the solution of the following saddle point problem

$$\begin{aligned} a(u, v) + b(v, \lambda) &= 0, \quad \forall v \in \tilde{\mathcal{V}} \\ b(u, \mu) &= 0, \quad \forall \mu \in \mathcal{M}. \end{aligned} \tag{3.27}$$

Because of the characterization of the space  $\mathcal{H}$ , it is possible to say that  $u \in \mathcal{H}$  solves problem (3.27). Now by letting  $v \in \mathcal{H}$  the variational formulation (3.27) can be rewritten as: find  $u \in \mathcal{H}$  such that,

$$a(u, v) = 0, \quad \forall v \in \mathcal{H}. \tag{3.28}$$

Note that problem (3.28) is the classic 2nd order elliptic problem with homogeneous Dirichlet boundary condition, and as a consequence  $u \in \mathcal{H}$  is the unique solution of both problems (3.28) and (3.27), see [19].

Now remain the issue of the uniqueness of the Lagrange multiplier, to prove it consider  $u \in \mathcal{H}$  solving problem (3.28) and that the following continuous linear functional on  $\tilde{\mathcal{V}}$  is satisfied in  $\mathcal{H}$ :

$$L \rightarrow -a(u, v), \tag{3.29}$$

then from equation (3.27)(a) it is possible to write,

$$b(v, \lambda) = -a(u, v), \quad \forall v \in \tilde{\mathcal{V}}. \tag{3.30}$$

As postulated  $-a(u, v)$  is satisfied in  $\mathcal{H}$ , therefore  $-a(u, v) = 0$ . By the Lemma 1 in Raviart and Thomas [19] page 393 there exist a unique  $\lambda \in \mathcal{M}$  satisfying equation (3.30). With this result, the existence and uniqueness of the solution  $(u, \lambda) \in (\tilde{\mathcal{V}} \times \mathcal{M})$  of the saddle point problem (3.27) is proved.

### 3.3 Finite element discretization

The discrete method to approximate the saddle point problem of the cell interface problem is based on problem (3.27) for proper conforming spaces  $\tilde{\mathcal{V}}_h \subset \tilde{\mathcal{V}}$  and  $\mathcal{M}_h \subset \mathcal{M}$ . Then,

the discrete problem is: find a pair  $(u_h, \lambda_h) \in (\tilde{\mathcal{V}}_h \times \mathcal{M}_h)$  such that:

$$\begin{aligned} a(u_h, v_h) + b(v_h, \lambda_h) &= 0, \quad \forall v \in \tilde{\mathcal{V}}_h \\ b(u_h, \mu_h) &= 0, \quad \forall \mu \in \mathcal{M}_h. \end{aligned} \quad (3.31)$$

An important difference between the discrete and continuous form of the saddle point problem is worth to mention here. For this, we introduce the discrete space  $\mathcal{H}_h$ ,

$$\mathcal{H}_h = \{v_h \in \tilde{\mathcal{V}}_h; b(v_h, \mu_h) = 0, \forall \mu_h \in \mathcal{M}_h\}. \quad (3.32)$$

The space  $\mathcal{H}_h$  may be considered an approximation of  $\mathcal{H}$ , however  $\mathcal{H}_h$  is not in general a conforming space of  $\mathcal{H}$ . The discrete version of the elliptic problem (3.28) is: find  $u_h \in \mathcal{H}_h$  such that

$$a(u_h, v_h) = 0, \quad \forall v_h \in \mathcal{H}_h, \quad (3.33)$$

Since in general  $\mathcal{H}_h \not\subset \mathcal{H}$ , the problem (3.33) is a non-conforming method to approximate problem (3.28). If  $(u_h, \lambda_h) \in \tilde{\mathcal{V}}_h \times \mathcal{M}_h$  is a solution of problem (3.31),  $u_h \in \mathcal{H}_h$  is a solution of problem (3.33) (see [19]). Moreover the following result is obtained:

**Theorem 3.3.** *If  $\|v_h\|_h^2 = a(v_h, v_h)$  is a norm over  $\mathcal{H}_h$ , then:*

1. *Problem (3.33) has a unique solution  $u_h \in \mathcal{H}_h$ ;*
2. *Problem (3.31) has a unique solution  $(u_h, \lambda_h) \in \tilde{\mathcal{V}}_h \times \mathcal{M}_h$  if and only if the following compatibility condition holds*

$$\{\mu_h \in \mathcal{M}_h; \forall v_h \in \tilde{\mathcal{V}}_h, b(v_h, \mu_h) = 0\} = \{0\} \quad (3.34)$$

The proof for the existence and uniqueness of the discrete problem can be found in [19].

### 3.3.1 The mortar finite element discretization

Here the notation used in the discrete HFEM or mortar finite element method with Lagrange multiplier is introduced. Consider a general non-overlapping domain partition of  $\Omega \in \mathbb{R}^2$  into polyhedral subdomains  $\Omega_k, 1 \leq k \leq K, \Omega = \bigcup_{k=1}^K \Omega_k$  with  $\Omega_l \cap \Omega_k = \emptyset, k \neq l$ , as shown in Figures 3.2 and 3.3

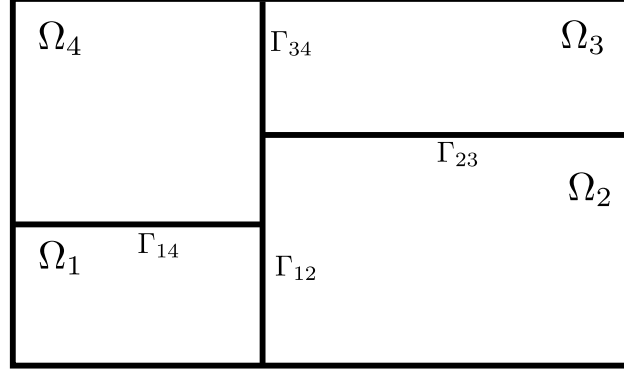


Figure 3.2: A general non overlapping domain decomposition

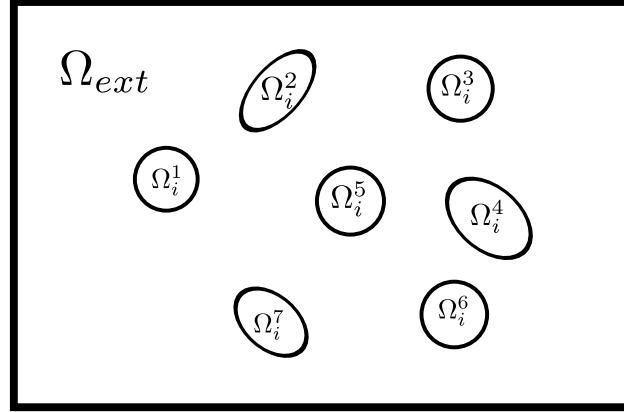


Figure 3.3: A domain decomposition that does not generate vertex

The set of vertices and edges of the subdomain  $\Omega_k$  are denoted by  $\mathcal{P}_{h_k}$  and  $\mathcal{E}_{h_k}$  respectively. Each subdomain  $\Omega_k$  will be associated with a family of shape regular simplicial triangulations  $\mathcal{T}_{h_k}$ . The interface between two subdomains is denoted by  $\bar{\Gamma}_{lk} = \bar{\Gamma}_{kl} := \partial\Omega_l \cap \partial\Omega_k$  and  $\mathbf{n}_{lk}$  will stand for the unit normal from  $\Omega_l$  toward  $\Omega_k$ . The union of all interfaces is called the skeleton of the domain  $S := \bigcup_{k,l=1}^K \bar{\Gamma}_{lk}$ . In each subdomain  $\Omega_k$  a conforming  $P_n$  finite element associated with the regular simplicial triangulation  $\mathcal{T}_{h_k}$  is defined. In general the domain discretization will not require that the triangulations  $\mathcal{T}_{h_i}$  and  $\mathcal{T}_{h_j}$  coincide on the interface  $\Gamma_{ij}$ . In the following,  $\mathcal{S}_n(\Omega_k; \mathcal{T}_{h_k})$  will denote the

standard conforming  $P_n$  Lagrange polynomial space of degree  $n \in \mathbb{N}$  associated to the triangulation  $\mathcal{T}_{h_k}$  defined in  $\Omega_k$ ,

$$\mathcal{S}_n(\Omega_k; \mathcal{T}_{h_k}) := \{u \in C(\Omega_k) : u|_T \in P_n(T), T \in \mathcal{T}_{h_k}, u|_{\Gamma_D} = \hat{u}\},$$

then the discrete global product space is defined as,

$$\tilde{\mathcal{V}}^{n,h}(\Omega) := \prod_{k=1}^K \mathcal{S}_n(\Omega_k; \mathcal{T}_{h_k}).$$

In general, the mortar finite element solution does not satisfy a pointwise continuity across the interface, instead some continuity condition has to be imposed either in terms of the Lagrange multiplier defined on the skeleton  $S$  or in terms of constraints on the space. In this work, the unconstrained mortar method with Lagrange multiplier was used which gives rise to a discrete saddle point problem. In the case of 2D problems, each interface  $\Gamma_{ij} = \Gamma_{ji}$ , inherits two 1D triangulations, one from  $\mathcal{T}_{h_i}$  and one from  $\mathcal{T}_{h_j}$ , without any restriction of generality, only one of the triangulations is used for the definition of the space of Lagrange multipliers, see Figure 3.4. The side where the Lagrange multiplier is defined is called the non-mortar side whereas the opposite side is called the mortar side. With this choice, the skeleton  $S$  of the domain can be uniquely decomposed into the union of the edges of the non-mortar sides of the decomposed domain.

The product space  $\mathcal{M}^{n,h}(S)$  of the Lagrange multiplier defined of the domain's skeleton  $S$  is now defined as:

$$\mathcal{M}^{n,h} := \prod_{i=1}^K \prod_{j \in M(i)} \mathcal{M}_n(\Gamma_{ij}; \mathcal{T}_{h_i}),$$

where

$$\begin{aligned} \mathcal{M}_n(\Gamma_{ij}; \mathcal{T}_{h_i}) := \{v \in C(\Gamma_{ij}) : v|_e \in P_n(e), \quad e \in \mathcal{E}_{h_i} \cap \Gamma_{ij}, \\ v|_e \in P_{n-1}(e) \text{ if } e \text{ contain an endpoint of } \Gamma_{ij}\}. \end{aligned}$$

From the definition of the Lagrange multiplier space note that the functions used to interpolate the discrete Lagrange multiplier  $\lambda_h$  are the same functions of  $v|_e$ . For the Lagrangian polynomial space  $P_n$  on triangular and quadrilateral elements, the interpolation function for the Lagrange multiplier match the classical hat functions with

compact support, see Figure 3.5. Since on the conservation problem treated in this work the domain partition into non-overlapping sets does not generate vertices, no modification of the interpolation space associated to the Lagrange multiplier is needed.

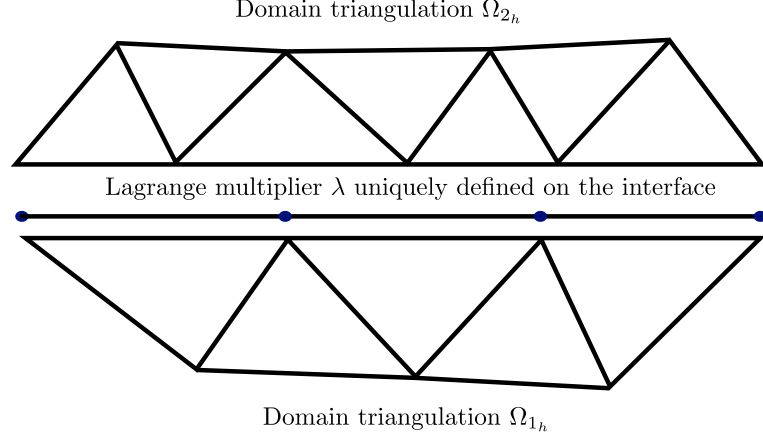


Figure 3.4: Triangulation in two non-overlapping domains and Lagrange multiplier triangulation defined on the non mortar side interface

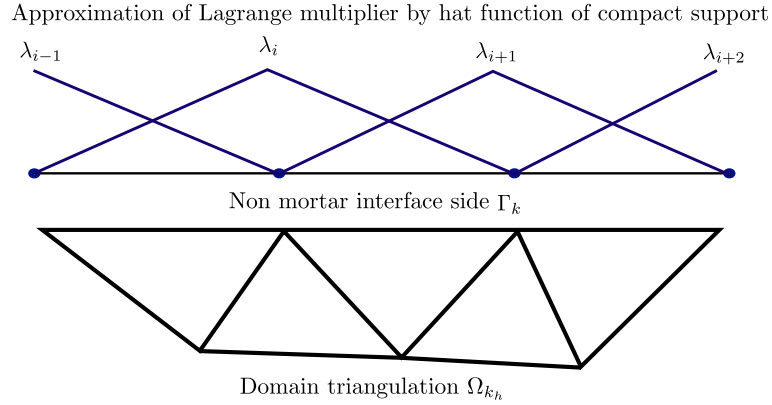


Figure 3.5: Triangulation of the Lagrange multiplier on the interface, and hat functions for interpolation of the approximated Lagrange multiplier.

The discrete mortar finite element problem is: find  $(u_h, \lambda_h) \in \tilde{\mathcal{V}}^{n;h} \times \mathcal{M}^{n;h}$  such that  $(u_h, \lambda_h)$  is the solution to the saddle point problem (3.31).

### 3.3.2 Error estimate

Here the error estimate in pertinent norm for the discrete problem is briefly presented. All the results presented here have been developed in [19, 21] and are based on the general Brezzi's theorem [43] for the existence and uniqueness of saddle point problems.

The error estimative for the non-conforming discrete variational problem, find  $u_h \in \mathcal{H}_h$

such that:

$$a(u_h, v_h) = \int_{\Omega} f v_h, \quad \forall v_h \in \mathcal{H}_h, \quad (3.35)$$

is presented in [21]. Assuming that the exact solution  $u \in H_0^1(\Omega)$  such that for any sub-domain  $k$  ( $1 \leq k \leq K$ ),  $u_k = u|_{\Omega_k} \in H^{n_k+1}(\Omega_k)$  the error estimative for the global problem in the  $L^2(\Omega)$  norm is:

$$\|u - u_h\|_{L^2(\Omega)} \leq C \sum_{k=1}^K h_k^{n_k+1} \|u_k\|_{H^{n_k+1}(\Omega_k)} \quad (3.36)$$

where  $n_k$  is the order of approximation of the partitioned sub-domain  $k$  and  $h_k = \max_{\kappa \in \mathcal{T}_{h_k}} h_{\kappa}$  with  $h_{\kappa}$  the measure of the edge of a triangle element. The numerical validation of the estimate (3.36) is present in section 5.1.

### 3.4 Time discretization for the transmembrane current

The general interface problem of the cell (3.21) is time dependent because of the response of the cell to an applied field. As mentioned in Section 2.1.1, the transmembrane current can be decomposed in two contributions, a capacitive and a ionic current:

$$I_m = C_m \frac{\partial V_m}{\partial t} + I_{ion}(V_m, \mathbf{q}), \quad \text{defined on } \Gamma. \quad (3.37)$$

The capacitive current is a consequence of the electric isolating property of the cell membrane, and for active cells as cardiac myocytes and neurons [15], the ionic current, is driven by the complex interactions between the main ionic currents of sodium, potassium and leakage currents described by the Hodgking-Huxley model [42]. In order to include the transmembrane current dynamics described by (3.37) into the problem of current flux conservation (3.21), the transmembrane potential  $V_m$  is written as an initial value problem,

$$C_m \frac{\partial V_m}{\partial t} = I_m - I_{ion}(V_m, \mathbf{q}), \quad \text{defined on } \Gamma, \quad (3.38)$$



where  $\mathbf{q}$  is a set of state variables describing the dynamics of the ionic currents. Note that  $V_m = u_i - u_e = [u]$  on  $\Gamma$ . An explicit time discretization is used to solve the initial value problem (3.38) and the following method to solve the boundary value problem (3.21) coupled with the initial value problem (3.38) is used, see [11].

The first step of the method is as follows: at  $t = 0$  solve the boundary value problem (3.39) with an initial value of  $V_m^t$  (the superscript  $t$  denotes the time dependency) to obtain  $(u_h, \lambda_h)$ ,

$$\begin{aligned} \int_{\Omega} \nabla u_h \cdot \nabla v_h dx + \int_{\Gamma} \lambda_h [v_h] ds &= 0, \quad \forall v \in \tilde{\mathcal{V}}_h \\ \int_{\Gamma} \mu_h [u_h] ds &= \int_{\Gamma} \mu_h V_m^t ds, \quad \forall \mu \in \mathcal{M}_h \end{aligned} \quad (3.39)$$

with  $\lambda_h = I_m$ , solve the initial value problem (3.38) with an explicit second order Runge-Kutta method to obtain a new value of the transmembrane potential  $V_m^t$  at an incremented time  $t + \delta t$ , the iterative process continue repeating the first step with the new value of the transmembrane potential  $V_m^{t+\delta t}$ , finishing once the computation time reached the aimed simulation time.

# 4 Computational aspects of the Saddle Point Problem

The variational formulation of the homogeneous interface problem was presented in the previous chapter, and the finite element space for the domain discretization was also introduced. In this chapter the computational details of the proposed discrete finite element method and the issues related to the solution of the associated saddle point problem of the electric response of the cell are discussed. More details can be found in [24, 22, 23].

## 4.1 Structure of the indefinite linear system

As mentioned in Section 3.3, the interface problem has a saddle point structure. Remember that the variational problem is: find a pair  $(u_h, \lambda_h) \in \tilde{\mathcal{V}}_h \times \mathcal{M}_h$  such that:

$$\begin{aligned} \int_{\Omega} \nabla u_h \cdot \nabla v_h dx + \int_{\Gamma} \lambda_h [v_h] ds &= 0, \quad \forall v \in \tilde{\mathcal{V}}_h \\ \int_{\Gamma} \mu_h [u_h] ds &= \int_{\Gamma} \mu_h V_m^t ds, \quad \forall \mu \in \mathcal{M}_h \end{aligned} \quad (4.1)$$

Since Lagrange polynomial spaces  $P_n$  are used to interpolate the solution  $u_h$  defined on the triangulation  $\mathcal{T}_{h_k}$  of each subdomain  $\Omega_k$ , the discrete problem (4.1) reduces to solve the following indefinite linear system

$$\begin{bmatrix} A & B \\ B^T & 0 \end{bmatrix} \begin{bmatrix} u \\ \lambda \end{bmatrix} = \begin{bmatrix} f \\ g \end{bmatrix}, \quad (4.2)$$

where the block matrix  $A$  is assembled from the contribution of  $\int_{\Omega} \nabla u_h \cdot \nabla v_h dx$ ,  $B$  from the contribution of  $\int_{\Gamma} \lambda_h [v_h] ds$ ,  $B^T$  is simply the transpose matrix of  $B$ ,  $f = 0$  and  $g$  is the load vector associated to the equation of the Lagrange multiplier assembled from the contribution of the term  $\int_{\Gamma} \mu_h V_m^t ds$ . In this work, the Lagrange multiplier defined on the interface triangulation is interpolated by classical hat functions. In this case the block

matrix  $B$  of equation 4.2 is sparse and is assembled by local contributions of mass matrices for one dimensional linear elements. For linear approximations these mass matrices have the typical structure:

$$M = \det(J) \begin{bmatrix} 1/3 & 1/6 \\ 1/6 & 1/3 \end{bmatrix}, \quad (4.3)$$

where  $J$  is the Jacobian matrix of the isoparametric mapping. This method may be extended to higher order approximations, in those cases the interface triangulation continue to inherit the interpolation of  $P_n(e)$ , and the local matrices contributions are square with dimension  $n + 1$  where  $n$  is the degree of the polynomial approximation. The indefinite linear system for the interface problem with two subdomains has the following structure:

$$\begin{bmatrix} A_{1,h} & 0 & B_{1,h} \\ 0 & A_{2,h} & B_{2,h} \\ B_{1,h}^T & B_{2,h}^T & 0 \end{bmatrix} \begin{bmatrix} u_i \\ u_e \\ \lambda \end{bmatrix} = \begin{bmatrix} 0 \\ 0 \\ V_m^t \end{bmatrix}, \quad (4.4)$$

where  $A_{1,h}$  and  $A_{2,h}$  are the stiffness matrices associated to the first and second subdomains respectively;  $B_{1,h}$  is the contribution to the Lagrange multiplier uniquely defined on the interface from the first domain and  $B_{2,h}$  the equivalent contribution from the second domain. Note that  $B_{1,h}^T$  and  $B_{2,h}^T$  has non null entries only where the domain triangulation coincide with the interface, therefore the matrices  $B_{1,h}^T$ ,  $B_{2,h}^T$  are highly sparse.

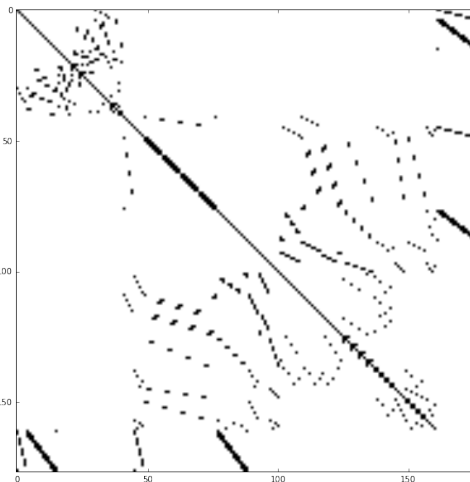


Figure 4.1: Sparsity pattern of the linear system associated to a discretization with triangular linear elements (161 nodes). Square matrix ( $177 \times 177$ ) with 929 non-zero entries and a maximum number of entries per row of 7.

In Figure 4.1 the sparsity pattern of the linear system associated to the finite element discretization, of two non-overlapping subdomains with triangular linear elements is shown.

## 4.2 Numerical methods to solve saddle point problems

A good deal of work has been devoted to study the properties of the linear system with the structure of equation (4.2) and the techniques to solve them [24]. Here, some of the basic methods are briefly described.

### 4.2.1 Schur Complement

One technique used to solve the linear system (4.2), is derived from the realization that the matrix  $K$ ,

$$K = \begin{bmatrix} A & B \\ B^T & 0 \end{bmatrix},$$

admits the following block triangular factorization

$$K = \begin{bmatrix} I & 0 \\ B^T A^{-1} & I \end{bmatrix} \begin{bmatrix} A & 0 \\ 0 & S \end{bmatrix} \begin{bmatrix} I & A^{-1} B \\ 0 & I \end{bmatrix} \quad (4.5)$$

where  $S = -B^T A^{-1} B$  is the Schur complement of  $A$  in  $K$ . Matrix  $K$  is not singular if and only if both matrices  $A$  and  $S$  are not singular, on the other hand the Schur complement matrix  $S$  is invertible if and only if the matrix  $B$  has full column rank, in that case  $S$  is symmetric negative definite. Under these conditions the problem (4.2) has a unique solution.

In practical terms, an immediate technique that can be used to compute  $u$  and  $\lambda$  from (4.2) given the block decomposition (4.5), is by the realization that given  $\lambda$ ,  $u$  can be written as

$$u = A^{-1}(f - B\lambda), \quad (4.6)$$

then upon the substitution of equation (4.6) in

$$B^T u = g, \quad (4.7)$$

the following linear system is obtained

$$B^T A^{-1} B \lambda = B^T A^{-1} f - g, \quad (4.8)$$

formed by the Schur complement matrix  $-S$  of  $A$ . Note that with this method we compute the solution  $\lambda$  and recover  $u$  by post-processing in (4.6). The main disadvantage of this method is the need of explicitly computing  $A^{-1}$  and the fact that even though  $S$  is symmetric definite, if the Dirichlet boundary conditions is imposed by penalization on  $A$  the associated Schur complement  $S$  is very ill conditioned. This situation gets even worse when the matrix  $B$  carries redundant information as may be the case when  $\lambda$  is interpolated by broken discontinuous functions on the interface. One possible form [24] to improve the global condition number of  $S$  is by realizing that the system (4.2) has a equivalent representation,

$$\begin{bmatrix} A + BWB^T & B \\ B^T & 0 \end{bmatrix} \begin{bmatrix} u \\ \lambda \end{bmatrix} = \begin{bmatrix} f + BWg \\ g \end{bmatrix}, \quad (4.9)$$

where  $g$  is the contribution of the jump in the general interface problem. The matrix  $W$  is a symmetric positive definite to be suitably defined. The simplest choice is to take  $W = \omega I$ ,  $\omega > 0$ . The objective is to obtain a better behaved Schur complement matrix  $S$  associated to the block  $A + BWB^T$ . In [24] it is recommended to chose  $\omega = \frac{\|A\|}{\|B\|^2}$ , however in this work this option was tested for the cell interface problem but this value is way to high to properly conditioning the Schur complement matrix  $S$ . A rather problem size dependent constant  $\omega$  that is four orders of magnitude lower than the proposed one was shown to be more effective to get a better conditioned system. This technique was needed to properly solve the interface cell problem with discontinuous interpolation of the Lagrange multiplier on the interface.

### 4.2.2 Penalty method

A solution method based on the Schur decomposition requires the inversion of the matrix  $A$  and, the solution of a possible ill conditioned symmetric system. A direct solver for the global system (4.5) such as Gauss elimination, requires pivoting techniques that destroys the symmetry of the system. An alternative problem can be derived to find an approximate solution of the original system. This is used in the following method, the general linear system associated to the cell interface problem is equivalent to finding the solution to the constrained minimization problem,

$$\min \mathcal{J}(u) = \frac{1}{2} u^T A u - f^T u, \quad (4.10)$$

Subject to  $Bu = g$ .

The following method is based on the observation that a solution  $x_*$  to (4.10) satisfies,

$$u_* = \lim_{\gamma \rightarrow \infty} u(\gamma)$$

where  $u(\gamma)$  is the unique solution of the unconstrained minimization problem:

$$\min \hat{\mathcal{J}}(u) = \mathcal{J}(u) + \frac{\gamma}{2} \|Bu - V_{m_t}\|^2. \quad (4.11)$$

If we define  $\lambda(\gamma) = \gamma(Bu(\gamma) - V_{m_t})$ , the associated linear system of the unconstrained minimization problem (4.11) can be written as:

$$\begin{bmatrix} A & B \\ B^T & -\epsilon I \end{bmatrix} \begin{bmatrix} u(\gamma) \\ \lambda(\gamma) \end{bmatrix} = \begin{bmatrix} f \\ V_{m_t} \end{bmatrix}, \quad \epsilon = \gamma^{-1} \quad (4.12)$$

It is possible to show that  $\|u(\gamma) - u_*\| = \mathcal{O}(\gamma^{-1})$  and the same for  $\|\lambda(\gamma) - \lambda_*\| = \mathcal{O}(\gamma^{-1})$  with  $\gamma \rightarrow \infty$ . See [24] and references therein. Now a direct solver based on a LU decomposition method may be used to solve (4.12).

### 4.2.3 *Krylov space method*

Methods to solve linear systems based on the computation of a sequence of candidate solutions are widely used. A family of methods based on this idea use constrained vectorial Krylov subspace to compute sequence of candidate solutions. For symmetric positive defined matrix the conjugate gradient method CG is the most used method in this context. A remarkable characteristic of the CG is its convergence rate, which in exact arithmetic warrant convergence of the solution in a maximum of  $n$  iterations where  $n$  is the dimension of the linear system.

In this work the linear system to be solved 4.2 is symmetric and positive indefinite, and in this case the CG can not be used, instead the Minimal Residual Method (MINRES) proposed and analysed by Paige [44], was used to approximate the solution to the saddle point problem 4.2. The MINRES method is based on the computation of candidate solutions sequences constrained with the orthogonality of the residual. In both methods the orthogonality is defined using the Euclidean inner product.

The development of this work was made over an existing FEM library (Cardiax) developed at the FISIOCOMP Laboratory [45]. Cardiax is constructed over PETSc [46] a specialized library for high performance scientific computation. The MINRES method available in PETSc together with a Jacobi preconditioner, was used to solve the saddle point linear system of the cell interface problem.

## 5 Results

In this chapter the numerical results of the interface cell problem are presented. First to validate the proposed numerical method, the  $h$ -convergence of the discrete MFEM is tested for a problem with known exact solution using a regular discretization of triangular elements; then the numerical and exact solution of cell polarization are compared for an isolated circular cell. The active response of the complex ionic current dynamics described by Hodgkin Huxley model is also solved. Finally the polarization process in a cell cluster is numerically investigated. Solutions with non matching grids are also presented.

### 5.1 $h$ -convergence of the method

In Section 3.3.2 the theoretical  $h$ -convergence rate of the mortar finite element was showed to be optimal in the  $L^2(\Omega)$  natural norm. To numerically evaluate this we propose to solve the following second order elliptic problem on  $\Omega = \Omega_1 \cup \Omega_2$ , with  $\Omega_2 = [-0.5, 0.5]^2$  and  $\Omega_1 = [-1.0, 1.0]^2 \setminus \Omega_2$  as shown in Figure 5.1 left,

$$\begin{aligned}
 -\kappa_1 \Delta u_1 &= f_1, & \in \Omega_1 \\
 -\kappa_2 \Delta u_2 &= f_2, & \in \Omega_2 \\
 u_1 &= 0, & \text{on } \partial\Omega_1 \\
 \nabla u_1 \cdot \mathbf{n} &= -\nabla u_2 \cdot \mathbf{n}, & \text{on } \Gamma \\
 u_1 - u_2 &= \sin(\pi x) \sin(\pi y), & \text{on } \Gamma
 \end{aligned} \tag{5.1}$$

where  $f_1 = f_2 = 4\pi^2 \sin(\pi x) \sin(\pi y)$ ,  $\kappa_1 = 1$ ,  $\kappa_2 = 2$  and the exact solution shown in Figure 5.1 right and given by:

$$\begin{aligned}
 u_1 &= 2 \sin(\pi x) \sin(\pi y), & \in \Omega_1 \\
 u_2 &= \sin(\pi x) \sin(\pi y), & \in \Omega_2.
 \end{aligned} \tag{5.2}$$



Following the procedure exposed in Section 3.3, the discrete version of the variational formulation of problem 5.1 can be loosely written,

$$\begin{aligned} \kappa \int_{\Omega} \nabla u_h \cdot \nabla v_h dx + \int_{\Gamma} \lambda_h [v_h] ds &= \int_{\Omega} f v_h dx, \quad \forall v_h \in \mathcal{X}_h \\ - \int_{\Gamma} \mu_h [u_h] ds &= \int_{\Gamma} \mu_h \sin(\pi x) \sin(\pi y) ds, \quad \forall \mu_h \in \mathcal{M}_h \\ u_1 &= 0, \quad \text{on } \Gamma_D \end{aligned} \quad (5.3)$$

with  $\kappa = (\kappa_1, \kappa_2)$ ,  $\Omega = \Omega_1 \cup \Omega_2$  and  $f = (f_1, f_2)$ .

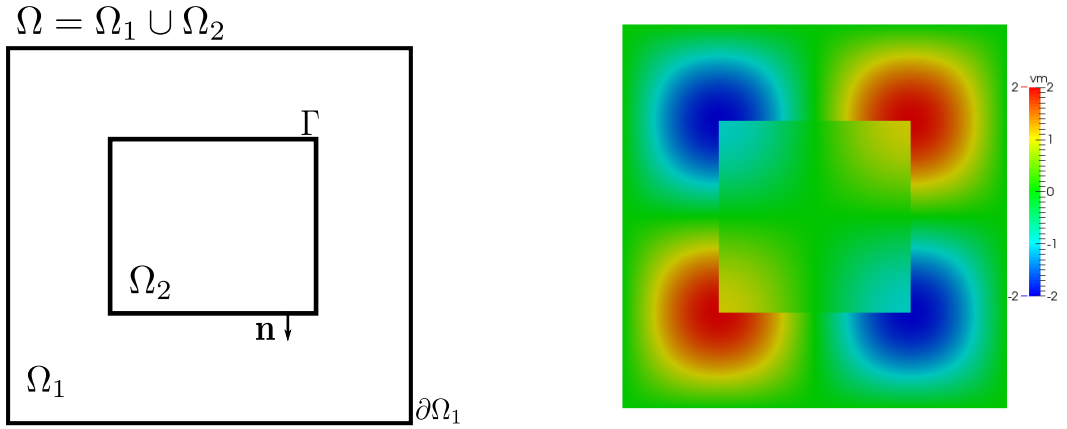


Figure 5.1: Computational domain and numerical solution of the second order interface problem.

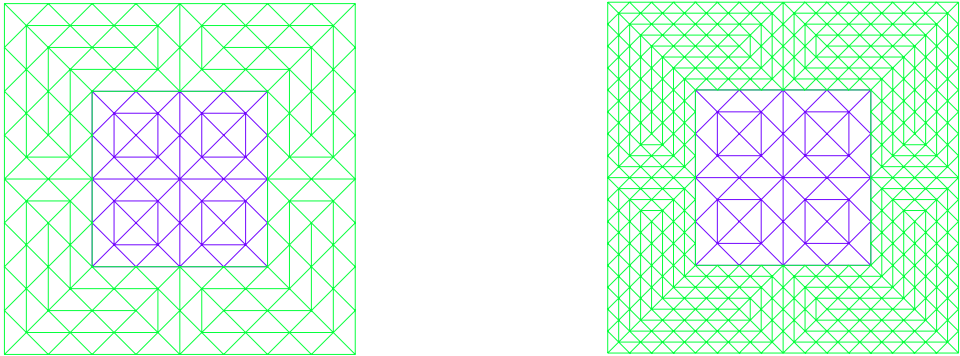


Figure 5.2: Domain discretization by triangular linear finite elements, matching discretization left and non-matching discretization at right.

The  $h$ -convergence of the MFEM, in  $L^2$  norm is tested for a domain discretization with triangular linear finite elements with matching and non-matching discretizations as shown in figure 5.2 left and right respectively. In Table 5.1 and 5.2, are listed the the error in  $L^2$  norm for the primal variable and the Lagrange multiplier for both cases.

	$\ u - u_h\ _{L^2(\Omega)}$		$\ \lambda - \lambda_h\ _{L^2(\Omega)}$	
<b>mesh</b>	<b>error</b>	<b>order</b>	<b>error</b>	<b>order</b>
16	1.12e-1	–	6.13e-1	–
32	3.48e-2	1.68	3.99e-1	0.62
64	9.24e-3	1.79	1.70e-1	0.93
128	2.36e-3	1.86	7.80e-2	1.02
256	5.96e-4	1.90	2.59e-2	1.15

Table 5.1:  $h$ -convergence order for the approximation of  $u_h$  and  $\lambda_h$  obtained by the MFEM for matching triangular elements.

	$\ u - u_h\ _{L^2(\Omega)}$		$\ \lambda - \lambda_h\ _{L^2(\Omega)}$	
<b>mesh</b>	<b>error</b>	<b>order</b>	<b>error</b>	<b>order</b>
24	6.79e-2	–	4.87e-1	–
48	2.23e-2	1.61	3.66e-1	0.89
96	6.20e-3	1.73	2.12e-1	1.05
192	1.61e-3	1.80	1.11e-1	1.09

Table 5.2:  $h$ -convergence order for the approximation of  $u_h$  and  $\lambda_h$  obtained by the MFEM for non-matching triangular elements.

In Figure 5.3 the  $h$ -convergence curves of the MFEM for matching (left) and non-matching (right) discretizations is depicted. As noted from the  $h$ -convergence test, the

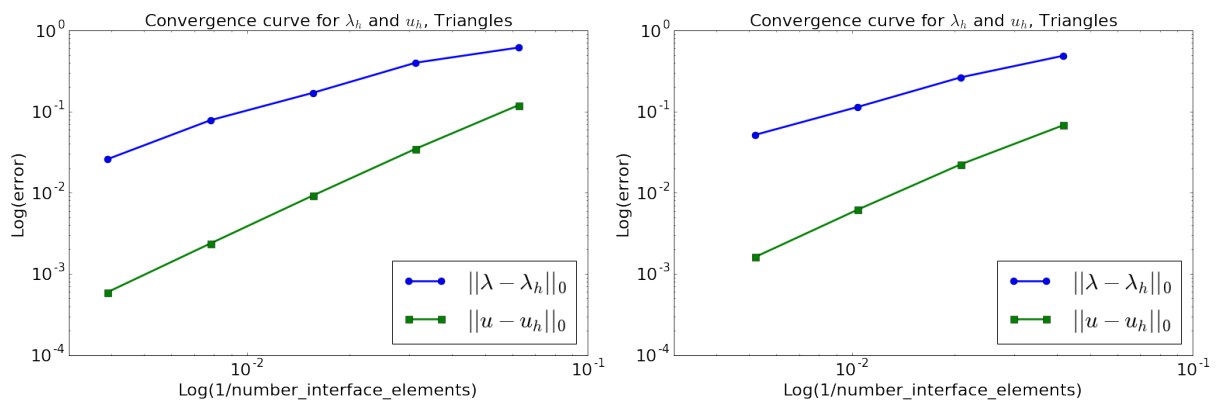


Figure 5.3:  $h$ -convergence study for the primal variable and the Lagrange multiplier for a triangular discretization with matching elements.

mortar finite element method with Lagrange multiplier to impose the interface condition, converges with optimal  $n + 1$  rate for the primal variable  $u_h$  presented in equation (4.1)

and with optimal rate  $n$  for the Lagrange multiplier  $\lambda_h$ . In the next section the cell polarization and the active response of the cell membrane is investigated with the MFEM with Lagrange multiplier.

## 5.2 Exact and numerical solution of the cell interface problem

As presented in Section 2.1.1, the response of an isolated circular cell to an applied electrical field is a two stage process. For a passive cell with idealized ionic current  $I_{ion} = \frac{V_m}{R_m}$  the representative time scale of the cell polarization process is in microseconds, and the exact solution to describe electric potential distribution inside and outside the cell is given by equation (2.7). This solution considers that the cell membrane acts as an electric insulator which makes the transmembranic current  $I_m$  to have two characteristics currents: a capacitive and the ionic current.

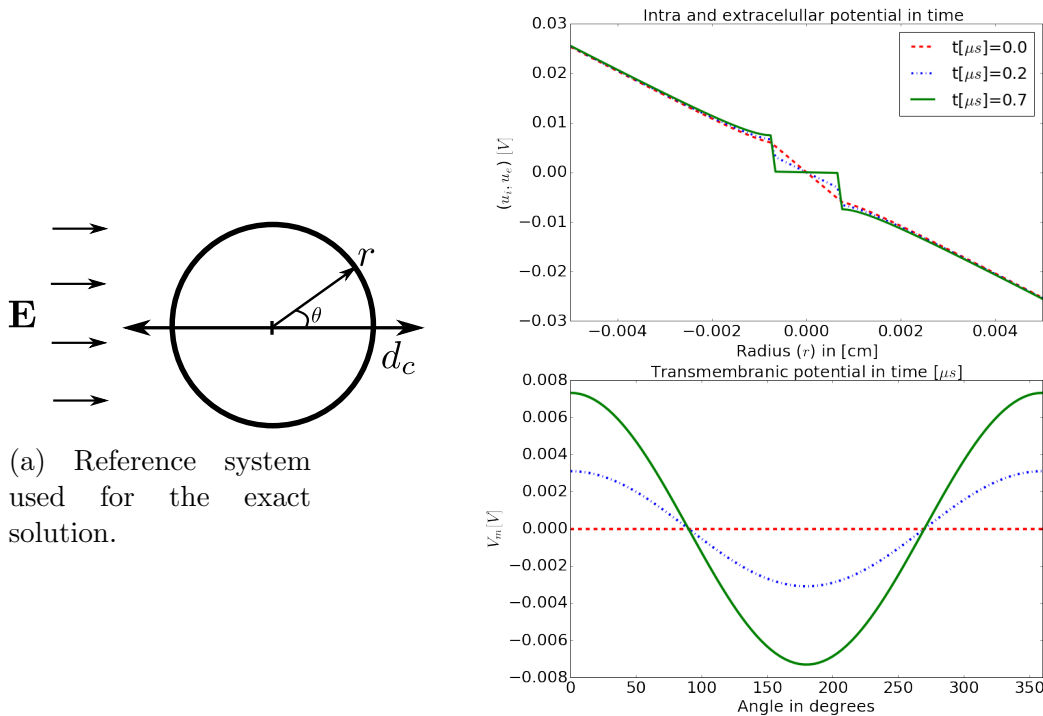


Figure 5.4: At left the circular cell and the reference system used in the exact solution, at top right the electric potential inside and outside the cell as function of the radius  $r$  for a fixed angle  $\theta = 0$ ; on the bottom right the transmembranic potential  $V_m = u_i - u_e$  defined on the cell interface as a function of the angular position  $\theta \in [0, 360]$ .

When the electric field  $\mathbf{E}$  is activated at  $t = 0$  the transmembranic potential  $V_m =$

$u_i - u_e$ , on  $\Gamma$  is zero, and the transmembrane current  $I_m = \lambda$  reaches its highest value. As mentioned in Section 3.4 the initial value problem for the transmembrane potential (3.38) is directly proportional to the transmembrane current  $I_m$ . For a passive cell with idealized ionic current  $I_{ion} = \frac{V_m}{R_m}$  the polarization process takes place at time scale of microseconds and finishes once the cell is totally polarized and equivalently the transmembrane current is zero. Figure 5.4 shows right the exact solution of the electric potential distribution at different time instants.

The exact solution presented in Figure 5.4 is for a circular cell of diameter  $d_c = 15[\mu m]$  the intra and extracellular conductance are  $\kappa_i = 5[\text{mS} \cdot \text{cm}^{-1}]$  and  $\kappa_e = 20[\text{mS} \cdot \text{cm}^{-1}]$ ; the membrane capacitance is  $C_m = 1[\mu\text{F} \cdot \text{cm}^{-2}]$ , the membrane resistance is  $R_m = 1\text{K}\Omega \cdot \text{cm}^2$ , the applied electric field is  $\mathbf{E} = 5\text{V} \cdot \text{cm}^{-1}$  and the transmembrane current is measured in  $I_m[\mu\text{A} \cdot \text{cm}^{-2}]$  to preserve dimensional consistency. As noted from Figure 5.4 right, at  $t = 0$  the transmembrane potential is zero and the electric potential distribution is uniform due to the capacitive characteristic of the membrane, the transmembrane potential increase proportionally to the transmembrane current, this causes the cell to create polar sides facing the cathode and anode of the electrodes applying the electric field. As the time passes the transmembrane current is consumed in form of potential difference between the intra and extracellular medium. The cell polarization finish once the transmembrane current is zero see Figure 5.5 and the transmembrane potential reach his highest and lowest value of around 0.008 and  $-0.008$  [V] respectively.

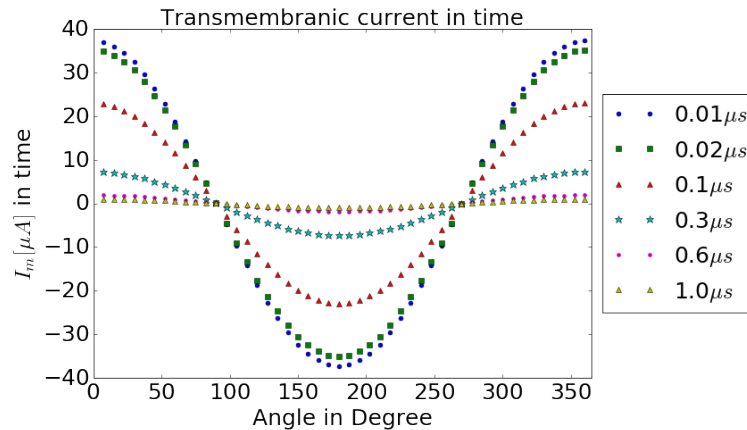


Figure 5.5: Transmembrane current in time.

Cell polarization process is numerically solved with the mortar finite element method proposed in section 3.3, the extracellular computational domain  $\Omega_e$  is considered big enough, such that the extracellular electric potential tends to the applied electric field

times the distance where the electrode is placed  $\hat{u} = -\mathbf{E} \cdot \mathbf{x}$  on the Dirichlet boundary condition  $\Gamma_D$ , see Figure 5.6. The distance between electrodes is 0.01[cm] and on the Neumann boundary side  $\Gamma_N$  a zero flux condition is imposed. A discretization was made with triangular elements generated using Gmsh [47] in two domains as shown in Figure 5.7.

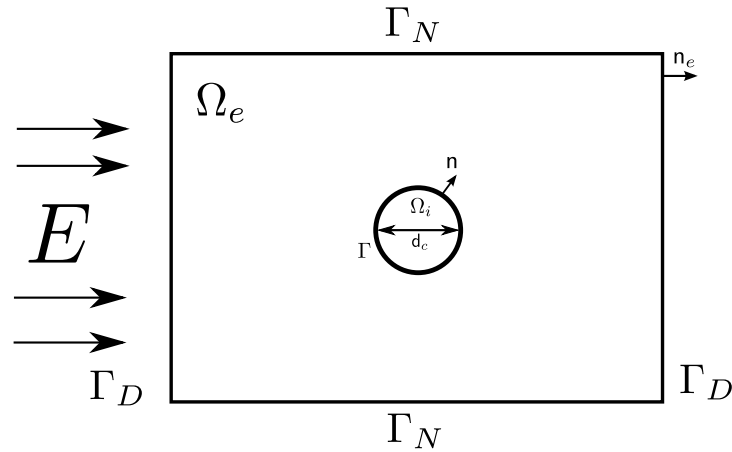


Figure 5.6: A circular cell in a conductive medium

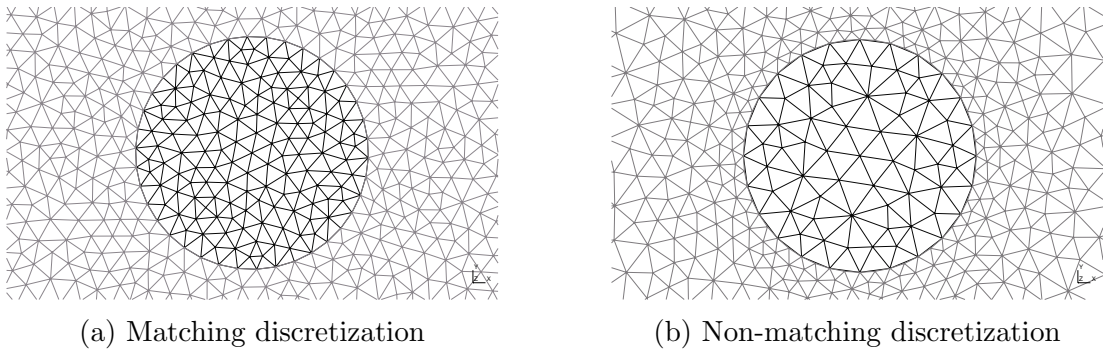


Figure 5.7: Cell domain discretization with triangular elements.

In Figure 5.5 the numerical transmembrane current  $I_m = \lambda$  is plotted as a function of the angle position of the cell considered as a circle. Note that conforming  $I_m$  goes to zero the transmembrane potential reaches the steady state condition and the cell polarization finishes. In Figure 5.9 the exact and numerical solution of the time evolution of the intra and extracellular electric potential and the transmembrane potential is evaluated as a function of the angle position  $\theta$ , see the reference system in Figure 5.8. Note that as time advances the transmembrane potential  $V_m$  change as the exact solution does. After  $1\mu s$  the cell is fully polarized, the transmembrane current is zero and the transmembrane potential reaches its highest and lowest value.

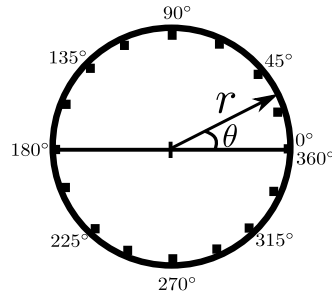


Figure 5.8: Reference system of the circular cell to plot the numerical and exact solution.

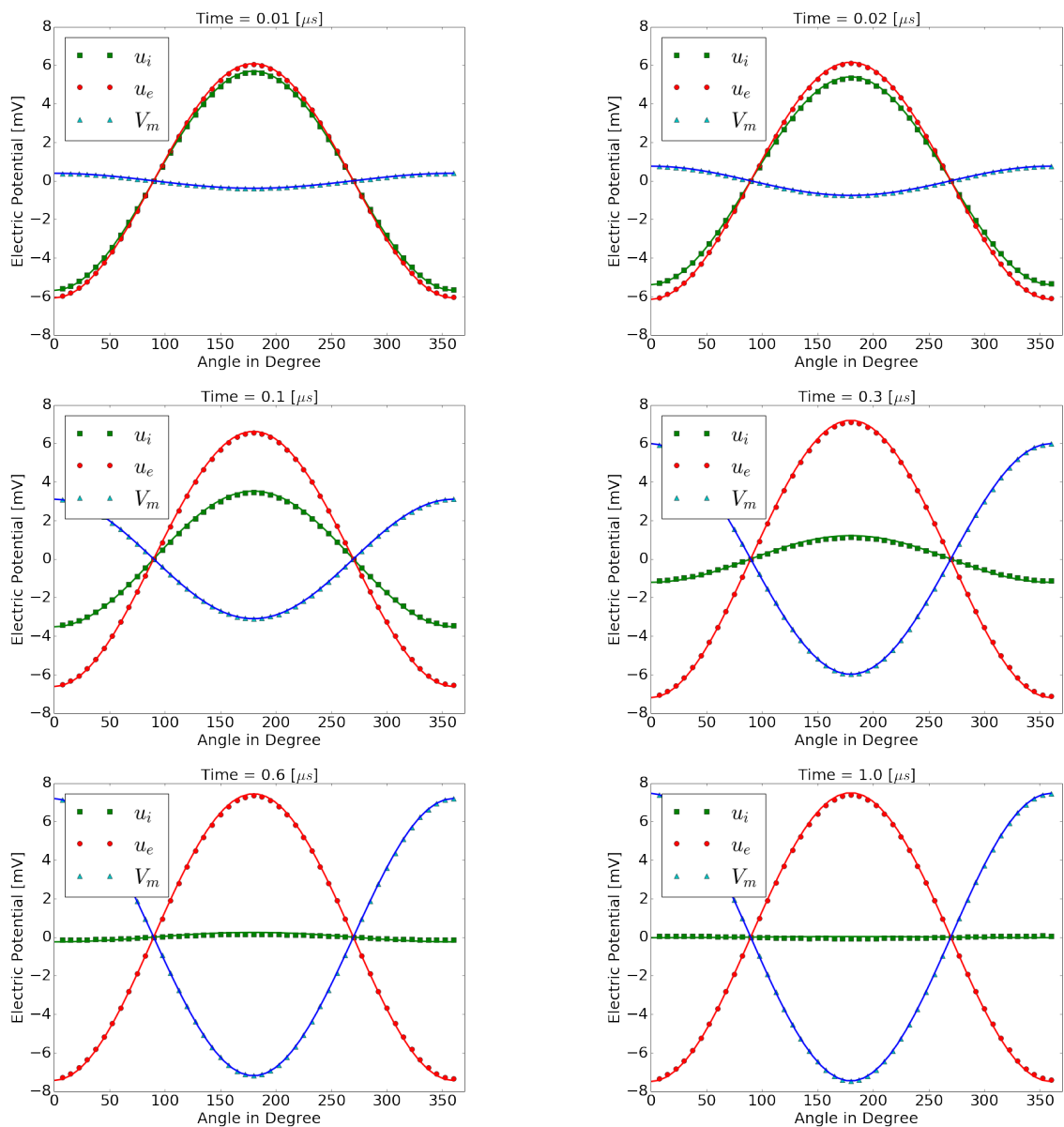


Figure 5.9: Electric potential in function of the angle evaluated at the membrane for the passive response of the cell with matching grids. Exact solution is plotted as continuous functions, and the numerical results are plotted as the dotted lines.

The iso-potential contour around and inside the circular cell in steady state of the

polarization process is presented in Figure 5.10.

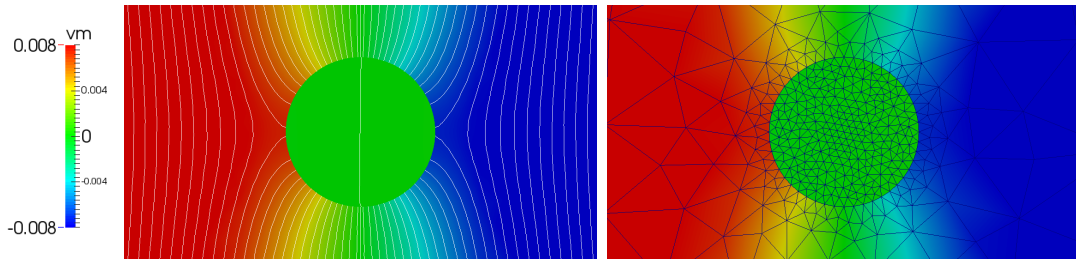


Figure 5.10: Left: steady state iso-potential contour around the cell. Right: the domain discretization by triangular elements used to solve the polarization process in the isolated cell. The distance between electrodes is  $0.01[\text{cm}]$ , the applied electric field is  $\mathbf{E} = 5[V \cdot \text{cm}^{-1}]$  and cell diameter is  $d_c = 15[\mu\text{m}]$ , the intra and extracellular conductivities are  $\kappa_i = 5[\text{mS} \cdot \text{cm}^{-1}]$  and  $\kappa_e = 20[\text{mS} \cdot \text{cm}^{-1}]$  respectively.

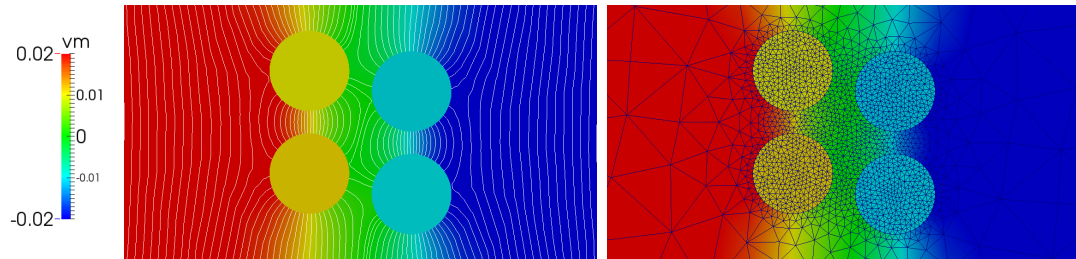


Figure 5.11: Left the iso-potential contour in a cluster of cells after  $1.0[\mu\text{s}]$  of simulation. Right: the matching domain discretization used to solve the polarization process in the cell cluster. The distance between electrodes is  $0.02[\text{cm}]$ , the applied electric field is  $\mathbf{E} = 5[V \cdot \text{cm}^{-1}]$  and cells diameter are  $d_c = 15[\mu\text{m}]$ , the intra and extracellular conductivities are the same as for isolated cell case.

Understanding the distribution of electric potential in a conductive medium in the presence of biological cells is important to understand the influence of applied electrical field in neurons activity [6, 14], and on the study of drugs supply into the cell's cytosol through electroporation [2]. With the presented numerical method the distribution of electric potential of a polarized cluster of cell can be numerically investigated see figure 5.11 and note the consistency with solutions presented in [11, 14].

### 5.3 Complex dynamics of the ion current and action potential

So far it was supposed that the initial conditions of the cell was a deviation of the rest potential or, equivalently, that the electric isolation property of the cell membrane was activated just after the electric potential  $\mathbf{E}$  was applied. In normal conditions, the transmembranic potential at rest of a biological cell is around  $-65[\text{mV}]$ , consequence of the different ion concentrations between the intra and extra cellular media, which is fundamental to warrant integrity of the cells structure; for detailed descriptions of the rest potential in biological cells see [15]. Due to this fact, in normal conditions the electric potential inside and outside the cell at rest ( $t = 0$ ) has a distribution similar to the one depicted in Figure 5.12.

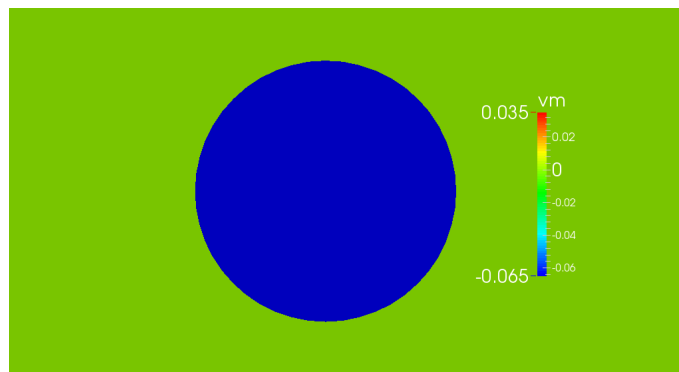


Figure 5.12: Circular biological cell with a transmembranic potential  $V_m = -65[\text{mV}]$  at rest ( $t = 0$ ).

After  $t > 0$  an external electric field  $\mathbf{E} = 10[\text{V}\cdot\text{cm}^{-1}]$  is applied and the active response, proper of neurons or cardiac myocytes take place in the time scale of milliseconds. Figure 5.13 shows the time evolution of the iso-potential contour of the active response of the cell in different time instants.



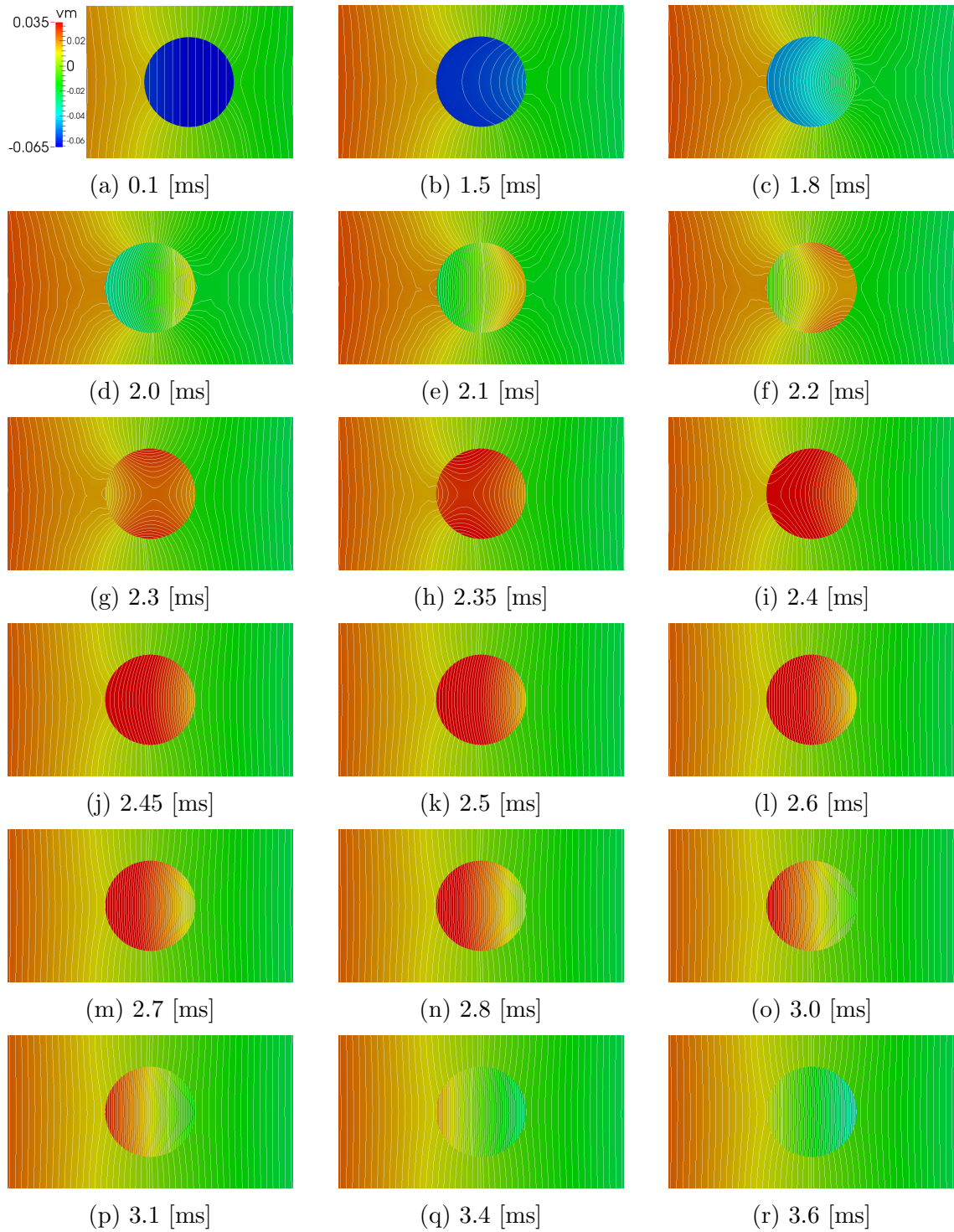


Figure 5.13: Distribution of the electric potential of the active response of a circular cell.

In Figure 5.14 the transmembrane potential  $V_m$ , the intra  $u_i$  and extracellular  $u_e$  potentials defined on the cell membrane (fixed  $r = \frac{d_c}{2}$  for different angular positions  $\theta$ ) is plotted in function of time.

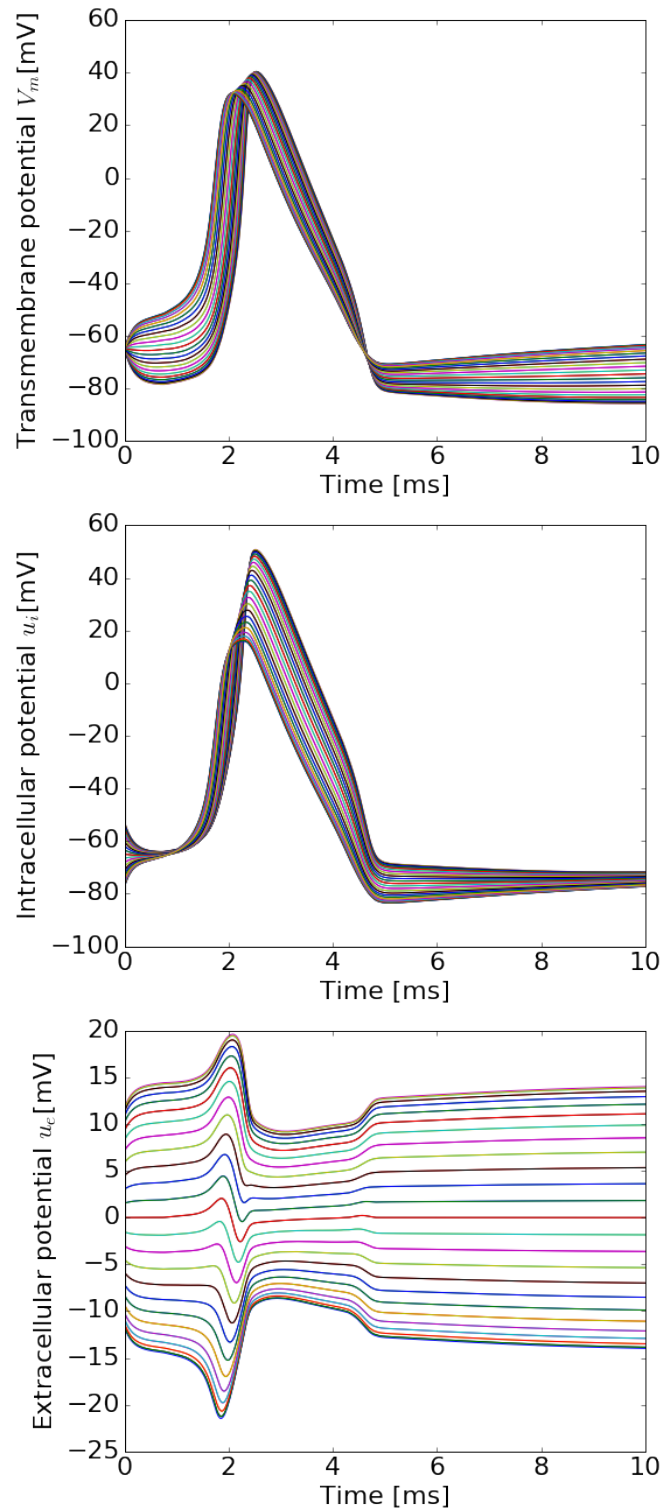


Figure 5.14: Active response of the cell to an applied electrical field of  $\mathbf{E} = 10[\text{V} \cdot \text{cm}^{-1}]$ . Each curve correspond with the time curse of electric potential in a fixed angular position ( $\theta$ ) at fixed radius  $r = \frac{d_c}{2}$ .

As noted in Figure 5.14 the active response of an isolated cell follows the typical curve of action potential [42, 15]. The parameters for the solution of the complex dynamics of ion currents were taken from [15] and correspond to the Hodgkin-Huxley model for the description of ionic current in squid giant axon. The numerical tool implemented in this work also described the behaviour of the active response when the stimulus is not high enough, for instance when an electric field  $\mathbf{E} = 6[\text{V} \cdot \text{cm}^{-1}]$  is applied at  $t > 0$  no action potential is triggered, which means that the transmembrane current due to the applied electrical field is not high enough to unchain the generation of an action potential on the cell, Figure 5.15 illustrate this situation.

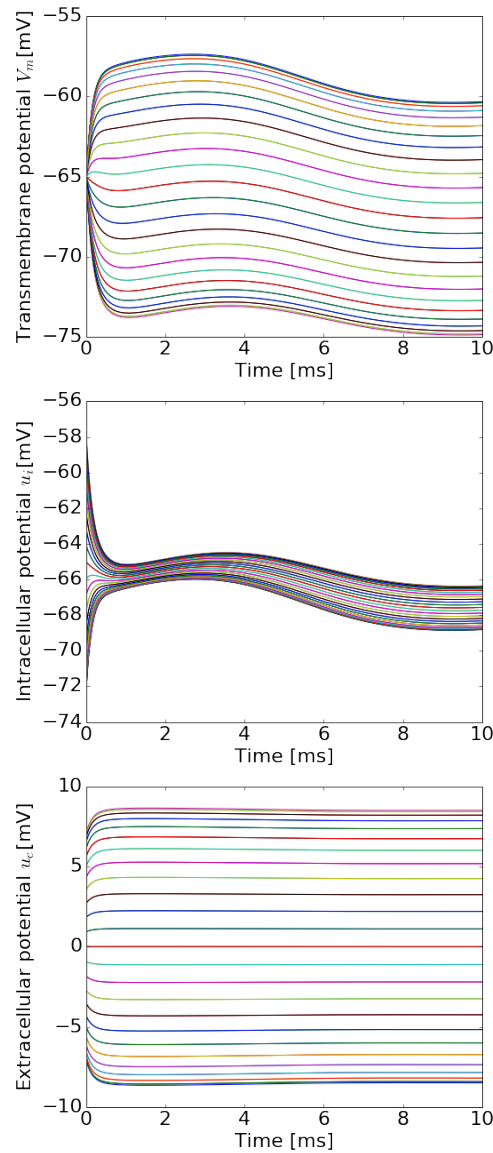


Figure 5.15: Response of the cell to an applied electrical field of  $\mathbf{E} = 6[\text{V} \cdot \text{cm}^{-1}]$ . Each curve correspond with the time course of electric potential in a fixed angular position on the cell interface.

We can also study the action potential unchained in a cluster of cells, see [14] for instance. In Figure 5.16 the time evolution of the iso-potential contour of the active response of a cluster of cells is presented for different time instants.

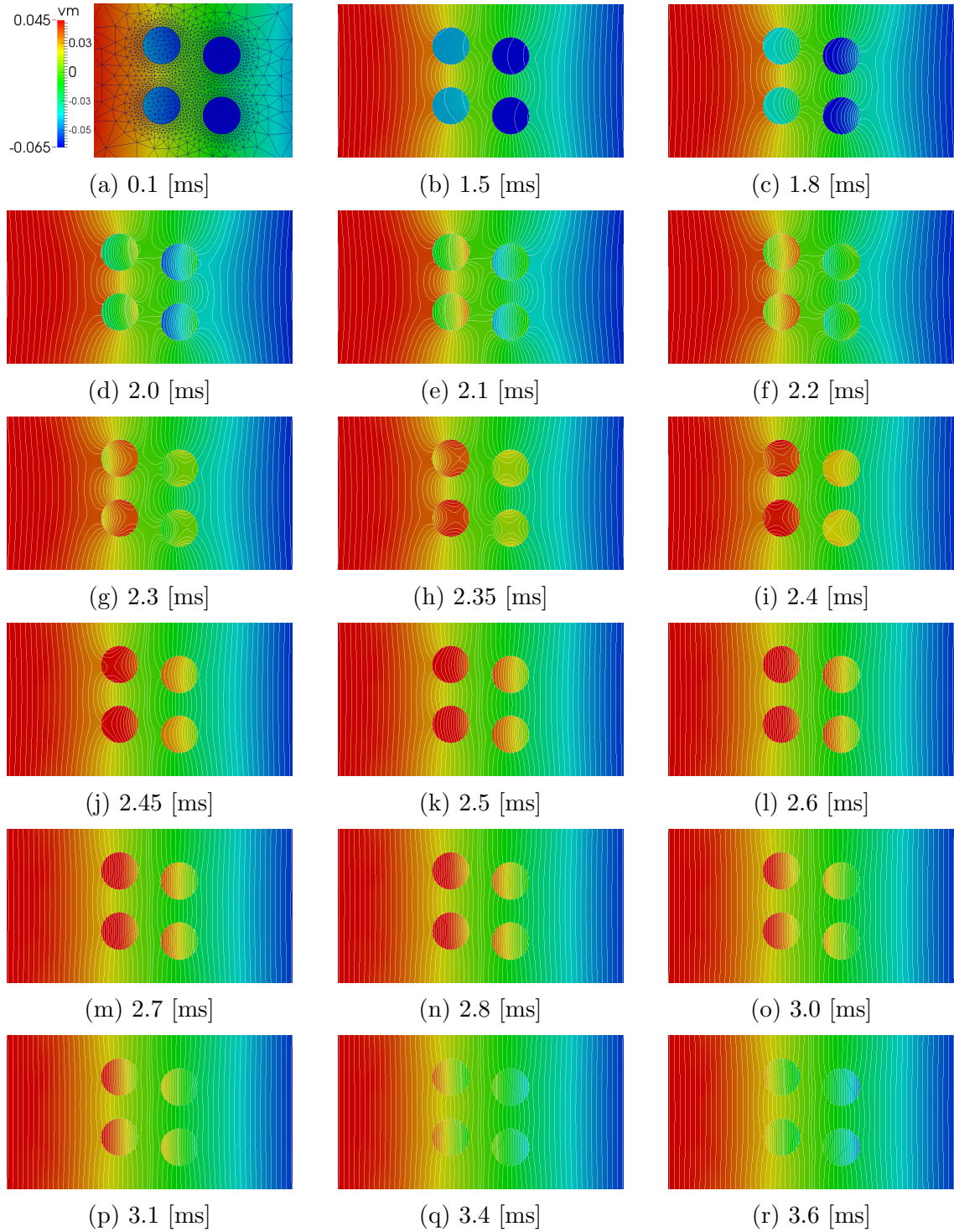


Figure 5.16: Distribution of the electric potential of the active response of cell cluster. At top left the used non-conforming domains discretization is shown. The distance between the cells at right and left is  $24 [\mu m]$ .

In Figure 5.17 the transmembrane potential  $V_m$ , the intra  $u_i$  and extracellular  $u_e$  potentials defined on the cell membrane of each cell, is plotted as a function of time.

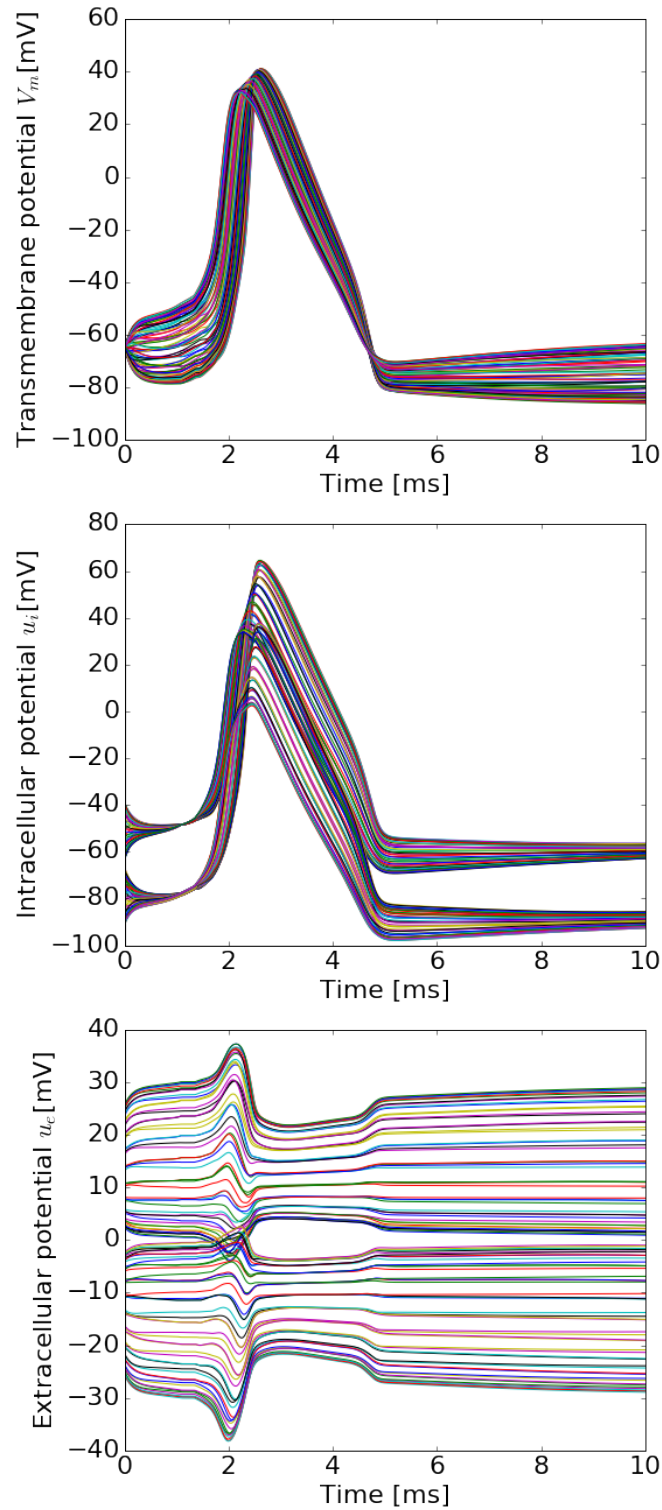


Figure 5.17: Active response of a cell cluster to an applied electrical field of  $\mathbf{E} = 20[\text{V} \cdot \text{cm}^{-1}]$ . Each curve correspond with the time course of electric potential in a fixed angular position on every cell interface.

## 6 Conclusions

In this work a Mortar Finite Element Method MFEM was effectively developed and used to numerically investigate the active and passive response of an isolated cell and cluster of cells to an applied electric field. The approximation properties of the MFEM were conforming with the results of the specialized literature, that is, optimal h-convergence order for the primal variable and the Lagrange multiplier for both the matching and non-matching domain discretization.

A hybrid variational formulation was effectively used to decoupled the boundary value problem describing the electric current conservation from the initial value problem describing the passive and the complex active response of the biological cell to applied field. The hybrid variational formulation effectively solved the cell interface problem, allowing to have discontinuous solutions in the computational domain without the need of having refined domain discretization to interpolate the solution. Therefore we conclude that the MFEM based on hybrid variational formulation is an elegant method to solve interface problems with complex dynamics.

The complex active response described by the Hodgkin-Huxley HH model of a cell and a cluster of cells to an applied electrical field was effectively solved via MFEM. It was found that the numerical tool reproduces the experimental behaviour in both cases, when the transmembranic current is high enough to generate action potential and also when it is not; due to the spatial resolution of the numerical tool a more detailed description of the action potential described by the HH model was obtained.

The most important product of this work is the extension of the Cardiac FEM library to solve second order heterogeneous interface problems with discontinuous solutions on the domain with conforming and non-conforming discretized domains via triangular finite elements.

During the development of this work, it was encountered that the Krylov subspace method MINRES together with a Jacobi preconditioner was the most robust method to solve the indefinite linear system associated to the discrete version of the saddle point problem encountered in the MFEM.

## 6.1 Future works

During the development of this work, alternative variational formulations were sketched on the paper but not implemented. In this sense, one possibility is to include GLS stabilization terms to the hybrid variational formulation, which generate a symmetric positive defined linear system suitable to solve with the conjugate gradient method or matrix decomposition methods as LU. Another interesting variational formulation appropriate for the cell interface problem, is a hybrid version of a mixed formulation. In theory this approach will allow to have optimal  $n + 1$  h-convergence for both the primal variable and the Lagrange multiplier, highly beneficial for the cell interface problem because of the improvement in the approximation order for the Lagrange multiplier used in the solution of the initial value problem. It is also proposed as future work the implementation of higher order mortar finite elements.

## REFERENCES

- [1] ORLOWSKI, S., MIR, L. M., “Cell electropermeabilization: a new tool for biochemical and pharmacological studies”, *Biochimica et Biophysica Acta (BBA)-Reviews on Biomembranes*, v. 1154, n. 1, pp. 51–63, 1993.
- [2] CHEN, C., SMYE, S., ROBINSON, M., EVANS, J., “Membrane electroporation theories: a review”, *Medical and Biological Engineering and Computing*, v. 44, n. 1, pp. 5–14, 2006.
- [3] ASHIHARA, T., YAO, T., NAMBA, T., ITO, M., IKEDA, T., KAWASE, A., TODA, S., SUZUKI, T., INAGAKI, M., SUGIMACHI, M., KINOSHITA, M., NAKAZAWA, K., “Electroporation in a Model of Cardiac Defibrillation”, *Journal of Cardiovascular Electrophysiology*, v. 12, n. 12, pp. 1393–1403, 2001.
- [4] KRASSOWSKA, W., “Effects of Electroporation on Transmembrane Potential Induced by Defibrillation Shocks”, *Pacing and Clinical Electrophysiology*, v. 18, n. 9, pp. 1644–1660, 1995.
- [5] NIKOLSKI, V. P., EFIMOV, I. R., “Electroporation of the heart”, *EP Europace*, v. 7, n. s2, pp. S146, 2005.
- [6] AGUDELO-TORO, A., NEEF, A., “Computationally efficient simulation of electrical activity at cell membranes interacting with self-generated and externally imposed electric fields”, *Journal of Neural Engineering*, v. 10, n. 2, pp. 026019, 2013.
- [7] KRASSOWSKA, W., NEU, J., “Response of a single cell to an external electric field”, *Biophysical Journal*, v. 66, n. 6, pp. 1768 – 1776, 1994.
- [8] GIMSA, J., WACHNER, D., “Analytical description of the transmembrane voltage induced on arbitrarily oriented ellipsoidal and cylindrical cells”, *Biophysical Journal*, v. 81, n. 4, pp. 1888–1896, 2001.
- [9] VALIČ, B., GOLZIO, M., PAVLIN, M., SCHATZ, A., FAURIE, C., GABRIEL, B., TEISSIÉ, J., ROLS, M.-P., MIKLAVČIČ, D., “Effect of electric field induced transmembrane potential on spheroidal cells: theory and experiment”, *European Biophysics Journal*, v. 32, n. 6, pp. 519–528, Oct 2003.



- [10] LEE, D. C., GRILL, W. M., “Polarization of a Spherical Cell in a Nonuniform Extracellular Electric Field”, *Annals of Biomedical Engineering*, v. 33, n. 5, pp. 603–615, 2005.
- [11] YING, W., HENRIQUEZ, C. S., “Hybrid finite element method for describing the electrical response of biological cells to applied fields”, *IEEE Transactions on Biomedical Engineering*, v. 54, n. 4, pp. 611–620, 2007.
- [12] PUCIHAR, G., MIKLAVČIČ, D., KOTNIK, T., “A time-dependent numerical model of transmembrane voltage inducement and electroporation of irregularly shaped cells”, *IEEE Transactions on Biomedical Engineering*, v. 56, n. 5, pp. 1491–1501, 2009.
- [13] SUSIL, R., ŠEMROV, D., MIKLAVČIČ, D., “Electric Field-Induced Transmembrane Potential Depends on Cell Density and Organizatio”, *Electro-and magnetobiology*, v. 17, n. 3, pp. 391–399, 1998.
- [14] YING, W., POURTAHERI, N., HENRIQUEZ, C. S., “Field stimulation of cells in suspension: use of a hybrid finite element method”. In: *Engineering in Medicine and Biology Society, 2006. EMBS’06. 28th Annual International Conference of the IEEE*, pp. 2276–2279, 2006.
- [15] KEENER, J., SNEYD, J., *Mathematical physiology: I: cellular physiology*. Springer Science & Business Media, 2010.
- [16] ŠEMROV, D., MIKLAVČIČ, D., “Numerical Modeling for In Vivo Electroporation”, In: JAROSZESKI, M. J., HELLER, R., GILBERT, R. (eds), *Electrochemotherapy, Electrogenetherapy, and Transdermal Drug Delivery: Electrically Mediated Delivery of Molecules to Cells*, pp. 63–81, Humana Press: Totowa, NJ, 2000.
- [17] CIARLET, P., KESAVAN, S., RANJAN, A., VANNINATHAN, M., *Lectures on the Finite Element Method. Lectures on mathematics and physics: Mathematics*, Tata Institute of Fundamental Research, 1975.

- [18] RAVIART, P.-A., THOMAS, J.-M., CIARLET, P. G., LIONS, J. L., *Introduction à l'analyse numérique des équations aux dérivées partielles*. v. 2. Dunod Paris, 1998.
- [19] RAVIART, P.-A., THOMAS, J., “Primal hybrid finite element methods for 2nd order elliptic equations”, *Mathematics of computation*, v. 31, n. 138, pp. 391–413, 1977.
- [20] BERNARDI, C., MADAY, Y., PATERA, A. T., “Domain Decomposition by the Mortar Element Method”, In: KAPER, H. G., GARBEY, M., PIEPER, G. W. (eds), *Asymptotic and Numerical Methods for Partial Differential Equations with Critical Parameters*, pp. 269–286, Springer Netherlands: Dordrecht, 1993.
- [21] BELGACEM, F. B., “The Mortar finite element method with Lagrange multipliers”, *Numerische Mathematik*, v. 84, n. 2, pp. 173–197, 1999.
- [22] WOHLMUTH, B. I., “A Mortar Finite Element Method Using Dual Spaces for the Lagrange Multiplier”, *SIAM Journal on Numerical Analysis*, v. 38, n. 3, pp. 989–1012, 2000.
- [23] LAMICHHANE, B. P., “Higher order mortar finite elements with dual Lagrange multiplier spaces and applications”, 2006.
- [24] BENZI, M., GOLUB, G. H., LIESEN, J., “Numerical solution of saddle point problems”, *Acta numerica*, v. 14, pp. 1–137, 2005.
- [25] BARBOSA, H. J., HUGHES, T. J., “The finite element method with Lagrange multipliers on the boundary: circumventing the Babuška-Brezzi condition”, *Computer Methods in Applied Mechanics and Engineering*, v. 85, n. 1, pp. 109–128, 1991.
- [26] BAIOCCHI, C., BREZZI, F., MARINI, L. D., “Stabilization of Galerkin methods and applications to domain decomposition”, In: BENSOUSSAN, A., VERJUS, J. P. (eds), *Future Tendencies in Computer Science, Control and Applied Mathematics: International Conference on the Occasion of the 25th*

*Anniversary of INRIA Paris, France, December 8–11, 1992 Proceedings*, pp. 343–355, Springer Berlin Heidelberg: Berlin, Heidelberg, 1992.

- [27] EWING, R. E., WANG, J., YANG, Y., “A stabilized discontinuous finite element method for elliptic problems”, *Numerical Linear Algebra with Applications*, v. 10, n. 1-2, pp. 83–104, 2003.
- [28] BRAESS, D., DAHMEN, W., WIENERS, C., “A Multigrid Algorithm for the Mortar Finite Element Method”, *SIAM Journal on Numerical Analysis*, v. 37, n. 1, pp. 48–69, 1999.
- [29] BREZZI, F., MARINI, L. D., “A three-field domain decomposition method”, *Contemporary Mathematics*, v. 157, pp. 27–27, 1994.
- [30] BERTOLUZZA, S., “Analysis of a mesh-dependent stabilization for the three fields domain decomposition method”, *Numerische Mathematik*, v. 133, n. 1, pp. 1–36, 2016.
- [31] RAVIART, P., THOMAS, J., “A mixed finite element method for 2-nd order elliptic problems”, *Mathematical aspects of finite element methods*, pp. 292–315, 1977.
- [32] BREZZI, F., FORTIN, M., *Mixed and Hybrid Finite Element Methods*. Springer-Verlag New York, Inc.: New York, NY, USA, 1991.
- [33] ARNOLD, D. N., BREZZI, F., “Mixed and nonconforming finite element methods : implementation, postprocessing and error estimates”, *ESAIM: M2AN*, v. 19, n. 1, pp. 7–32, 1985.
- [34] BABUŠKA, I., “The Finite Element Method with Penalty”, *Mathematics of Computation*, v. 27, n. 122, pp. 221–228, 1973.
- [35] NITSCHKE, J., “Über ein Variationsprinzip zur Lösung von Dirichlet-Problemen bei Verwendung von Teilräumen, die keinen Randbedingungen unterworfen sind”. In: *Abhandlungen aus dem mathematischen Seminar der Universität Hamburg*, v. 36, n. 1, pp. 9–15, 1971.
- [36] ARNOLD, D. N., BREZZI, F., COCKBURN, B., MARINI, L. D., “Unified Analysis of Discontinuous Galerkin Methods for Elliptic Problems”, *SIAM Journal on Numerical Analysis*, v. 39, n. 5, pp. 1749–1779, 2002.

- [37] COCKBURN, B., “Discontinuous Galerkin Methods for Convection-Dominated Problems”, In: BARTH, T. J., DECONINCK, H. (eds), *High-Order Methods for Computational Physics*, pp. 69–224, Springer Berlin Heidelberg: Berlin, Heidelberg, 1999.
- [38] COCKBURN, B., GOPALAKRISHNAN, J., LAZAROV, R., “Unified Hybridization of Discontinuous Galerkin, Mixed, and Continuous Galerkin Methods for Second Order Elliptic Problems”, *SIAM Journal on Numerical Analysis*, v. 47, n. 2, pp. 1319–1365, 2009.
- [39] EGGER, H., “A class of hybrid mortar finite element methods for interface problems with non-matching meshes, 2009”, *Preprint: AICES-2009-2*.
- [40] ARRUDA, N. C., LOULA, A. F., ALMEIDA, R. C., “Locally discontinuous but globally continuous Galerkin methods for elliptic problems”, *Computer Methods in Applied Mechanics and Engineering*, v. 255, n. Supplement C, pp. 104 – 120, 2013.
- [41] PLONSEY, R., HEPPNER, D. B., “Considerations of quasi-stationarity in electrophysiological systems”, *The bulletin of mathematical biophysics*, v. 29, n. 4, pp. 657–664, Dec 1967.
- [42] HODGKIN, A. L., HUXLEY, A. F., “A quantitative description of membrane current and its application to conduction and excitation in nerve”, *The Journal of Physiology*, v. 117, n. 4, pp. 500–544, 1952.
- [43] BREZZI, F., “On the existence, uniqueness and approximation of saddle-point problems arising from lagrangian multipliers”, *ESAIM: Mathematical Modelling and Numerical Analysis - Modélisation Mathématique et Analyse Numérique*, v. 8, n. R2, pp. 129–151, 1974.
- [44] PAIGE, C. C., SAUNDERS, M. A., “Solution of sparse indefinite systems of linear equations”, *SIAM journal on numerical analysis*, v. 12, n. 4, pp. 617–629, 1975.
- [45] CAMPOS, J. O., W. DOS SANTOS, R., SUNDNES, J., ROCHA, B. M., “Preconditioned Augmented Lagrangian formulation for nearly incompressible

cardiac mechanics”, *International Journal for Numerical Methods in Biomedical Engineering*, cnm.2948.

- [46] BALAY, S., ABHYANKAR, S., ADAMS, M. F., BROWN, J., BRUNE, P., BUSCHELMAN, K., DALCIN, L., EIJKHOUT, V., GROPP, W. D., KAUSHIK, D., KNEPLEY, M. G., MCINNES, L. C., RUPP, K., SMITH, B. F., ZAMPINI, S., ZHANG, H., ZHANG, H., “PETSc Web page”, <http://www.mcs.anl.gov/petsc>, 2016.
- [47] GEUZAINÉ, C., REMACLE, J.-F., “Gmsh: A 3-D finite element mesh generator with built-in pre-and post-processing facilities”, *International journal for numerical methods in engineering*, v. 79, n. 11, pp. 1309–1331, 2009.